ADVANCES IN ATMOSPHERIC SCIENCES, VOL. 39, JUNE 2022, 903–926

• Original Paper •

Evaluation of Arctic Sea Ice Drift and its Relationship with Near-surface Wind and Ocean Current in Nine CMIP6 Models from China

Xiaoyong YU*[1,2], Chengyan LIU[2], Xiaocun WANG[3], Jian CAO[4], Jihai DONG[3], and Yu LIU[5]

[1]*Binjiang College*, *Nanjing University of Information Science and Technology*, *Wuxi* 214105, *China*

[2]*Southern Marine Science and Engineering Guangdong Laboratory (Zhuhai)*, *Zhuhai* 519082, *China*

[3]*School of Marine Sciences*, *Nanjing University of Information Science and Technology*, *Nanjing* 210044, *China*

[4]*School of Atmospheric Sciences*, *Nanjing University of Information Science and Technology*, *Nanjing* 210044, *China*

[5]*Marine Science and Technology College*, *Zhejiang Ocean University*, *Zhoushan* 316022, *China*

(Received 28 April 2021; revised 4 November 2021; accepted 15 November 2021)

ABSTRACT

The simulated Arctic sea ice drift and its relationship with the near-surface wind and surface ocean current during 1979–2014 in nine models from China that participated in the sixth phase of the Coupled Model Intercomparison Project (CMIP6) are examined by comparison with observational and reanalysis datasets. Most of the models reasonably represent the Beaufort Gyre (BG) and Transpolar Drift Stream (TDS) in the spatial patterns of their long-term mean sea ice drift, while the detailed location, extent, and strength of the BG and TDS vary among the models. About two-thirds of the models agree with the observation/reanalysis in the sense that the sea ice drift pattern is consistent with the near-surface wind pattern. About the same proportion of models shows that the sea ice drift pattern is consistent with the surface ocean current pattern. In the observation/reanalysis, however, the sea ice drift pattern does not match well with the surface ocean current pattern. All nine models missed the observational widespread sea ice drift speed acceleration across the Arctic. For the Arctic basin-wide spatial average, five of the nine models overestimate the Arctic long-term (1979–2014) mean sea ice drift speed in all months. Only FGOALS-g3 captures a significant sea ice drift speed increase from 1979 to 2014 both in spring and autumn. The increases are weaker than those in the observation. This evaluation helps assess the performance of the Arctic sea ice drift simulations in these CMIP6 models from China.

Key words: Arctic sea ice, sea ice drift, CMIP6, model evaluation

Citation: Yu, X. Y., C. Y. Liu, X. C. Wang, J. Cao, J. H. Dong, and Y. Liu, 2022: Evaluation of Arctic sea ice drift and its relationship with near-surface wind and ocean current in nine CMIP6 models from China. *Adv. Atmos. Sci.*, **39**(6), 903–926, https://doi.org/10.1007/s00376-021-1153-4.

Article Highlights:

- Simulations of Arctic sea ice drift and its relationship with near-surface wind and surface current in nine CMIP6 models from China are evaluated for the period of 1979–2014.
- Most of the nine models can reasonably represent the observational Beaufort Gyre and Transpolar Drift Stream in the climatological sea ice drift field.
- It is still challenging for most of these models to capture the observational seasonal evolution and long-term trend in the Arctic sea ice drift speed.

1. Introduction

Arctic sea ice is a vital component of the Earth's climate system (de Vernal et al., 2020). In addition to the coverage and thickness, the drift of Arctic sea ice is also of substantial research interest because of its important roles in Arctic climate, such as regulating ice mass distribution and atmosphere–ocean energy exchange (Kwok et al., 2013). The drift of Arctic sea ice has two large-scale patterns: the Beaufort Gyre (BG) and the Transpolar Drift Stream (TDS) (e.g., Colony and Thorndike, 1984). Arctic sea ice drift also exhibits significant seasonality, with maximum speed in September/October and minimum speed in March/April

* Corresponding author: Xiaoyong YU
Email: xiaoyong.yu@nuist.edu.cn

(Rampal et al., 2009; Olason and Notz, 2014). As Arctic sea ice extent has decreased rapidly in recent decades (e.g., Stroeve et al., 2012; Serreze and Stroeve, 2015), the sea ice tends to move faster (Rampal et al., 2009; Spreen et al., 2011; Kwok et al., 2013; Zhang et al., 2021). Although it is clear that Arctic sea ice moves in response to atmospheric forcing (e.g., Vihma et al., 2012; Lei et al., 2019; Zhang et al., 2021), Rampal et al. (2009) found that the substantial increase in the Arctic spatially averaged sea ice drift speed (+17% per decade for winter and +8.5% for summer, based on buoy observation) from 1979 to 2007 is more likely caused by decreased sea ice mechanical strength instead of increased atmospheric forcing. Vihma et al. (2012) confirmed the finding in Rampal et al. (2009) that atmospheric forcing cannot explain the increasing trend of Arctic spatially averaged sea ice drift speed during a similar time (1989–2009). The changes in Arctic sea ice drift and its driver are not regionally uniform. Based on satellite data, Spreen et al. (2011) showed that the winter Arctic sea ice drift speed trend for the period 1992–2009 varies between −4% and 16% per decade depending on the location. Increasing wind speed may explain part of the observed increase in drift speeds in the Central Arctic, but thinning of the sea ice is a more likely cause of sea ice drift acceleration in other regions (Spreen et al., 2011). Kwok et al. (2013) showed the BG and the TDS were enhanced during 1982–2009, especially during the last decade. Based on a longer period (1980–2013) and focused over the Canadian Basin, Petty et al. (2016) also showed the strengthening of the BG and proposed several mechanisms to explain the change, such as ice strength reduction (which is caused by declines in ice thickness and concentration), changes to the ice morphology, the atmospheric boundary layer stability, and/or geostrophic currents.

For information on how Arctic sea ice will change in the future, we rely on predictions and projections from climate models. Therefore, it is vital to know whether climate models can properly capture observed historical sea ice drift and its dependency on atmospheric and oceanic forcing and sea ice conditions. Rampal et al. (2011) examined Arctic sea ice simulation in the models that participated in the third phase of the Coupled Model Intercomparison Project (CMIP3) and showed that these models failed to capture the observed seasonal cycle and the acceleration of Arctic sea ice drift in recent decades. Based on the fifth phase of the Coupled Model Intercomparison Project (CMIP5) models, Tandon et al. (2018) found that only a few models captured the observed seasonal cycle of sea ice drift speed. Among the state-of-art global climate models that participated in the sixth phase of the Coupled Model Intercomparison Project (CMIP6), 13 are from China (Zhou et al., 2019). Their performance on simulating Arctic sea ice concentration, area, extent, thickness, volume, and mass budget and snow depth on the ice under modern climate conditions is examined in recent multi-model (Davy and Outten, 2020; Notz et al., 2020; Shu et al., 2020; Smith et al., 2020; Årthun et al., 2021; Chen et al., 2021; Keen et al., 2021; Long et al., 2021; Shen et al., 2021) and single model (Guo et al., 2020a; Wang et al., 2020; Ren et al., 2021; Rong et al., 2021) evaluation studies. Notz et al. (2020) and Long et al. (2021) showed that BCC-CSM2-MR, FGOALS-f3-L, and FIO-ESM-2-0 are able to simultaneously simulate a plausible amount of Arctic sea-ice loss and a plausible change in global mean temperature over time. In addition, Long et al. (2021) found that CAMS-CSM1-0 largely underestimates the Arctic sea ice extent decline, and BCC-CSM2-MR, CASM-CSM1-0, and FGOALS-f3-L obviously overestimate the climatological sea ice concentration over the Barents Sea and East Greenland Sea. Shen et al. (2021) and Rong et al. (2021) confirmed the underestimation of the Arctic sea ice extent decline in CAMS-CSM1-0. Guo et al. (2020a) confirmed the overestimated climatological sea ice concentration over the Barents Sea and East Greenland Sea in FGOALS-f3-L. Ren et al. (2021) and Wang et al. (2020) pointed out that the underestimation of climatological sea ice concentration over the Barents Sea and East Greenland Sea in BCC-CSM2-MR may be caused by the underestimated surface net radiation and heat transport from the Atlantic Ocean. Smith et al. (2020) reported that BCC-CSM2-MR and BCC-ESM1 overestimated the Arctic sea ice melt-period and underestimated the freeze-up and closing period. Cao et al. (2018) demonstrated that NESM3 can represent the modern Arctic climate well, while a cold bias exists over the Barents Sea. However, the performance of these models in simulating the Arctic sea ice drift is unknown so far. Therefore, this study aims to extend the current evaluation studies by providing evaluation of Arctic sea ice drift and its relationship with near-surface wind and surface ocean current in the historical runs of the CMIP6 models from China. This paper is organized in the following way: section 2 describes the model characteristics and the observational data as well as the analysis methods used; section 3 presents the evaluation of spatial patterns in simulated Arctic sea ice drift climatology and trends and the relationship of these patterns with those in Arctic near-surface wind and surface ocean current; evaluation of the seasonal evolution and trend in the simulated Arctic basin-wide mean sea ice drift speed, near-surface wind speed, and surface ocean current is given in section 4; section 5 presents the summary and conclusions.

2. Data and method

2.1. *Model data*

We evaluate nine coupled models (BCC-CSM2-MR, BCC-ESM1, CAMS-CSM1-0, CAS-ESM2-0, CIESM, FGOALS-f3-L, FGOALS-g3, FIO-ESM-2-0, and NESM3) from China that participated in the CMIP6. We only investigate 9 of 13 models from China because the other 4 models (BCC-CSM2-HR, BNU-ESM-1-1, FGOALS-f3-H, and TaiESM1) have not provided the sea ice drift vector in their

CMIP6 historical experiments on the ESGF CMIP6 data distribution website yet. Table 1 shows that only two different sea ice models are used in these coupled models: Sea Ice Simulator (SIS) and Los Alamos sea ice model (CICE). BCC-CSM2-MR and BCC-ESM1 use the SIS, and the other seven coupled models use the CICE. More detailed information about these coupled models can be found in Table 1. The monthly sea ice drift, near-surface wind, and surface ocean current vectors from the CMIP6 historical experiments of these nine models are selected for evaluation in this study. As the near-surface wind vector (CMIP6 standard name uas, vas) in CIESM, FGOALS-g3, and FIO-ESM-2-0 are not provided, the wind vector at 1000 hPa is used instead in these three models. The data from the first ensemble member of each model and for the period of 1979–2014 (36 years) is used. We focus the evaluation on spring and autumn when sea ice usually reaches the maximum and minimum extent, respectively.

2.2. *Datasets for evaluation*

For the evaluation of the simulated Arctic sea ice drift, the NSIDC-0116 Polar Pathfinder (referred to as NSIDC Pathfinder hereafter) daily sea ice motion vectors (https://nsidc.org/data/NSIDC-0116/versions/3) are used. This dataset provides daily sea ice motion vectors derived from a wide variety of sensors in both gridded and non-gridded (raw) files. We selected the daily sea ice motion vector that was projected on the 25 km EASE-grid and merged observations from a variety of sensors over the Northern Hemisphere. As we use the monthly sea ice drift vectors to obtain the sea ice drift magnitude and direction in the nine CMIP6 models, the monthly sea ice drift vector components in NSIDC Pathfinder are calculated accordingly to assess the observational sea ice drift magnitude and direction. Previous evaluation studies (Sumata et al., 2014, 2015; Gui et al., 2020) show that the bias of NSIDC Pathfinder sea ice drift speed in summer is larger than that in winter, and the summer Arctic average sea ice drift speed is obviously underestimated. These studies also show that the larger the sea ice drift speed or lower the sea ice concentration, the larger the absolute error in sea ice drift. More detail about this dataset can be found in Tschudi et al. (2016). The NSIDC Pathfinder is used in this study because only this product provides the full-season, long-term (1979–2014) sea ice

Table 1. Characteristics of the nine CMIP6 models from China.

Model	Atmosphere (lon × lat)	Ocean (lon × lat)	Sea ice (lon × lat)	Reference
BCC-CSM2-MR	BCC-AGCM3-MR	MOM4-L40v2	SISv2	
	(1) T106, 46 layers (2) Top at 1.459 hPa	(1) 1° × 1° (1°/3 between 30°S–30°N), 40 layers	(1) 1° × 1° (1°/3 between 30°S–30°N)	(Wu et al., 2019)
BCC-ESM1	BCC-AGCM3-Chem	MOM4-L40v2	SISv2	
	(1) T42 (~2.8° × 2.8°), 26 layers (2) Top at 2.917 hPa	(1) 1° × 1° (1°/3 between 30°S–30°N), 40 layers	(1) 1° × 1° (1°/3 between 30°S × 30°N)	(Wu et al., 2020)
CAMS-CSM1-0	ECHAM5(v5.4)	MOM4	SIS	
	(1) T106,31 lyears (2) Top at 10 hPa	(1) 1° × 1° (1°/3 between 10°S–10°N), 50 layers		(Rong et al., 2018)
CAS-ESM2-0	IAP-AGCM 5.0	LICOM2.0	CICE4.0	
	(1) 1.41° × 1.42°, 35 layers (2) top at 2.2 hPa	(1) 1° × 1° (0.5°–1° between 20°S–20°N), 30 layers		(Jin et al., 2021)
CIESM	CIESM-AM1.0	CIESM-OM1.0	CICE4	
	(1) 1° × 1°, 30 layers (2) top at 1 hPa	1° × 1°; 60 levels		(Lin et al., 2020)
FGOALS-f3-L	FAMIL	LICOM3	CICE4.0	
	(1) C96 (1° × 1°), 32 layers (2) top at 2.16 hPa	primarily 1°; 362 × 196 longitude/latitude; 30 levels		(Guo et al., 2020b)
FGOALS-g3	GAMIL3	LICOM3	CICE4.0	
	~2° × 2°	1° (increased to be 0.5° at equator), 30 layers	1° (increased to be 0.5° at equator)	(Pu et al., 2020)
FIO-ESM-2-0	CAM5	POP2	CICE4.0	
	(1) f09 (0.9° × 1.25°), 30 layers, Top at 2.25 hPa	(1) 1.1° × (0.27°–0.54°), 61 layers	(1) 1.1° × (0.27°–0.54°)	(Bao et al., 2020)
NESM3	ECHAM v6.3	NEMO v3.4	CICE v4.1	
	(1) ~1.9° × 1.9°, 47 layers, top at 0.01 hPa	(1) 1° × 1°, 46 layers	(1) 1° × 0.5°, 5 layers (4 layers of sea ice and 1 layer of snow on the top)	(Cao et al., 2018)

drift data over the whole Arctic so far. This advantage enables us to evaluate the climatology and trend of Arctic sea ice drift in the models during different seasons.

For the near-surface wind, the monthly 10-m wind from ERA-Interim (referred to as ERA-I hereafter) with 1° × 1° horizontal resolution is used. Compared with the daily average 10-m wind speed from the North Pole drifting ice stations of the former Soviet Union, Lindsay et al. (2014) found that the monthly mean bias of daily averaged 10-m wind speed in ERA-Interim is mostly less than 0.5 m s^{-1}. Besides, the ERA-Interim wind speed has the best correlation (higher than 0.85) with the observation among six atmospheric reanalysis products (Lindsay et al., 2014). More information about this dataset is given by Berrisford et al. (2011). For the surface ocean current, we use the monthly surface ocean current from Ocean Reanalysis System 4 (ORAS4) with 1° × 1° horizontal resolution. Detailed information about ORSA4 is given by Balmaseda et al. (2013). Caution is necessary when using these two reanalysis products because of the sparse observation over the Arctic Ocean.

2.3. *Method*

2.3.1. *Spatial average*

For the calculations of Arctic basin-wide mean sea ice drift, near-surface wind, and surface ocean current, we follow the method of Olason and Notz (2014) and Docquier et al. (2017) by using the Scientific Ice Expeditions (SCICEX) box (Rothrock et al., 2008) as the domain for the spatial average. The domain of the SCICEX box is shown in Fig. 1a.

2.3.2. *Trends*

Since sea ice drift, near-surface wind, and surface ocean current are vectors, the changes of sea ice drift, near-surface wind, and surface ocean current could happen in their magnitude or direction, or both. Therefore, we calculate not only the trends of the sea ice drift, near-surface wind, and surface ocean current magnitude, but also the trends of their vector components when we evaluate the spatial patterns of the sea ice drift, near-surface wind, and surface ocean current changes over the Arctic. The trends of their vector components are then used to compose a trend vector that shows the direction of their change. For the evaluation of the Arctic basin-wide mean sea ice drift change, we only calculate the trend of the sea ice drift magnitude. The two-tailed Student's t-test is used to perform the significance test for the trend. A trend with a confidence level equal to or higher than 95% is considered significant.

3. Spatial patterns of Arctic sea-ice drift, near-surface wind, and ocean current

3.1. *Spatial patterns of Arctic sea ice drift*

The spatial patterns of spring (March-April-May; MAM) long-term (1979–2014) mean sea ice drift direction (vector) and speed (shading) in the observation and models are shown in Fig. 1. In the NSIDC Pathfinder, the spring sea ice drift pattern is characterized by a typical BG, in which sea ice moves anticyclonically over the Amerasian basin, and a typical TDS, in which there is sea ice drift from the Siberian coast all the way to the Fram Strait (Fig. 1a). All nine models capture the BG and TDS in the spring sea ice drift pattern except for NESM3, in which there are three small anticyclonic vortices aligned together instead of a BG in the sea ice drift field over the Amerasian basin. This distinct sea ice drift pattern in NESM3 (Fig. 1j) is linked to the ocean current beneath the sea ice (see section 3.2). The exact extent, location, and strength of BG and TDS vary among the models. The BG and TDS in CAMS-CSM1-0, CIESM, FGOALS-f3-L, and FIO-ESM-2-0 are close to those in the observation. In BCC-CSM2-MR and FGOALS-g3, however, the simulated BG and TDS are different from those in the observation. The BG extent in BCC-CSM2-MR is smaller than that in the observation. The TDS is curved instead of straight, as in the observation. Consequently, in BCC-CSM2-MR, the sea ice over the Siberian coast first drifts toward the Canadian Archipelago and north of Greenland and then turns to drift toward the Fram Strait and the water between Svalbard and the Franz Josef Land (Fig. 1b). The cyclonic near-surface wind centered near the Barents/Kara Sea may be the driver of the curved sea ice drift (see section 3.2 for detail). The BG in FGOALS-g3 is much smaller and weaker than that in the observation. The simulated TDS starts not just from the Siberian coast, but also from the Beaufort Sea. This makes the TDS in FGOALS-g3 much wider than that in the observation. Also, the simulated TDS is weaker and its axis is tilted more eastward compared to that in the observation. In BCC-ESM1, the bias of the simulated TDS is very close to that in BCC-CSM2-MR. This could be because both BCC-ESM1 and BCC-CSM2-MR used the same sea ice model. In CAS-ESM2-0, the BG and TDS are both interrupted by the data void at the North Pole (Fig. 1e). Near there, the sea ice drifts around the data void. This is because the sea ice grid in CAS-ESM2-0 filtered the data near the North Pole, so the North Pole acts as an artificial island for the sea ice (Sun and Zhou, 2010; Xu et al., 2013). The simulated TDS in NESM3 is narrower than that in the observation.

In autumn, the observational extent of the BG is smaller and its shape is more asymmetrical compared to that in spring (Fig. 2a). Meanwhile, the TDS is curved instead of straight. Of the nine models, two of them (CAS-ESM2-0 and FGOALS-g3) show BG extents similar to the BG extent in the observation; five of them (BCC-CSM2-MR, BCC-ESM1, CAMS-CSM1-0, FGOALS-f3-L, and FIO-ESM-2-0) simulate a larger and stronger BG than that in the observation; two of them (NESM3 and CIESM) do not capture the BG. For TDS simulation, four of the nine models (BCC-CSM2-MR, BCC-ESM1, CAS-ESM2-0, and FGOALS-g3) simulate a curved TDS. However, the curved TDS in CAS-ESM2-0 is caused by the "artificial island" near the North Pole, and the direction of the curve is different from that in the observation. Another four models (CAMS-CSM1-0,

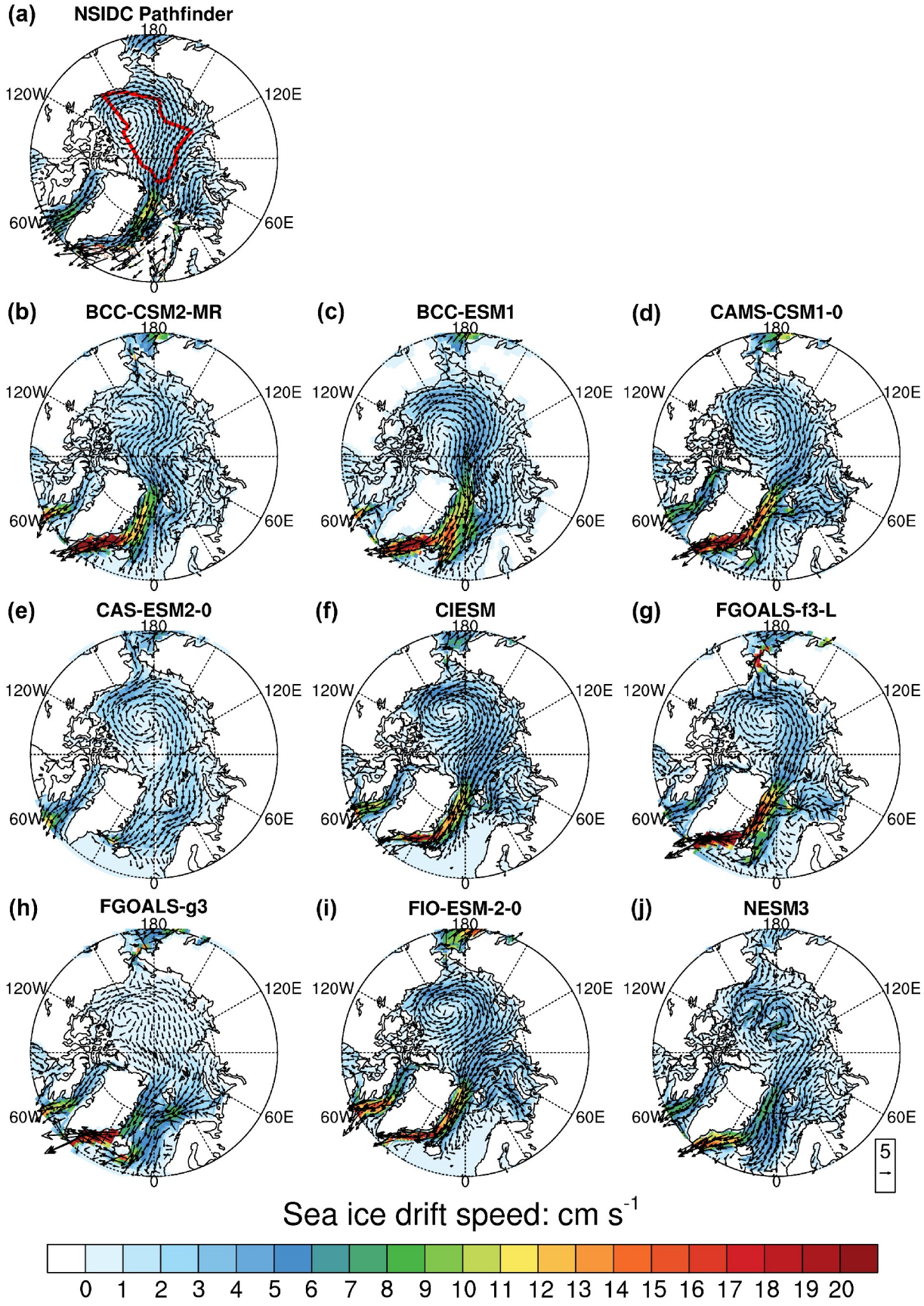

Fig. 1. Spatial pattern of the spring (MAM) long-term (1979–2014) mean sea ice drift direction (vector) and speed (shading) in NSIDC Polar Pathfinder and nine CMIP6 models (BCC-CSM2-MR, BCC-ESM1, CAMS-CSM1-0, CAS-ESM2-0, CIESM, FGOALS-f3-L, FGOALS-g3, FIO-ESM-2-0, and NESM3) from China. The SCICEX domain is marked as the red box.

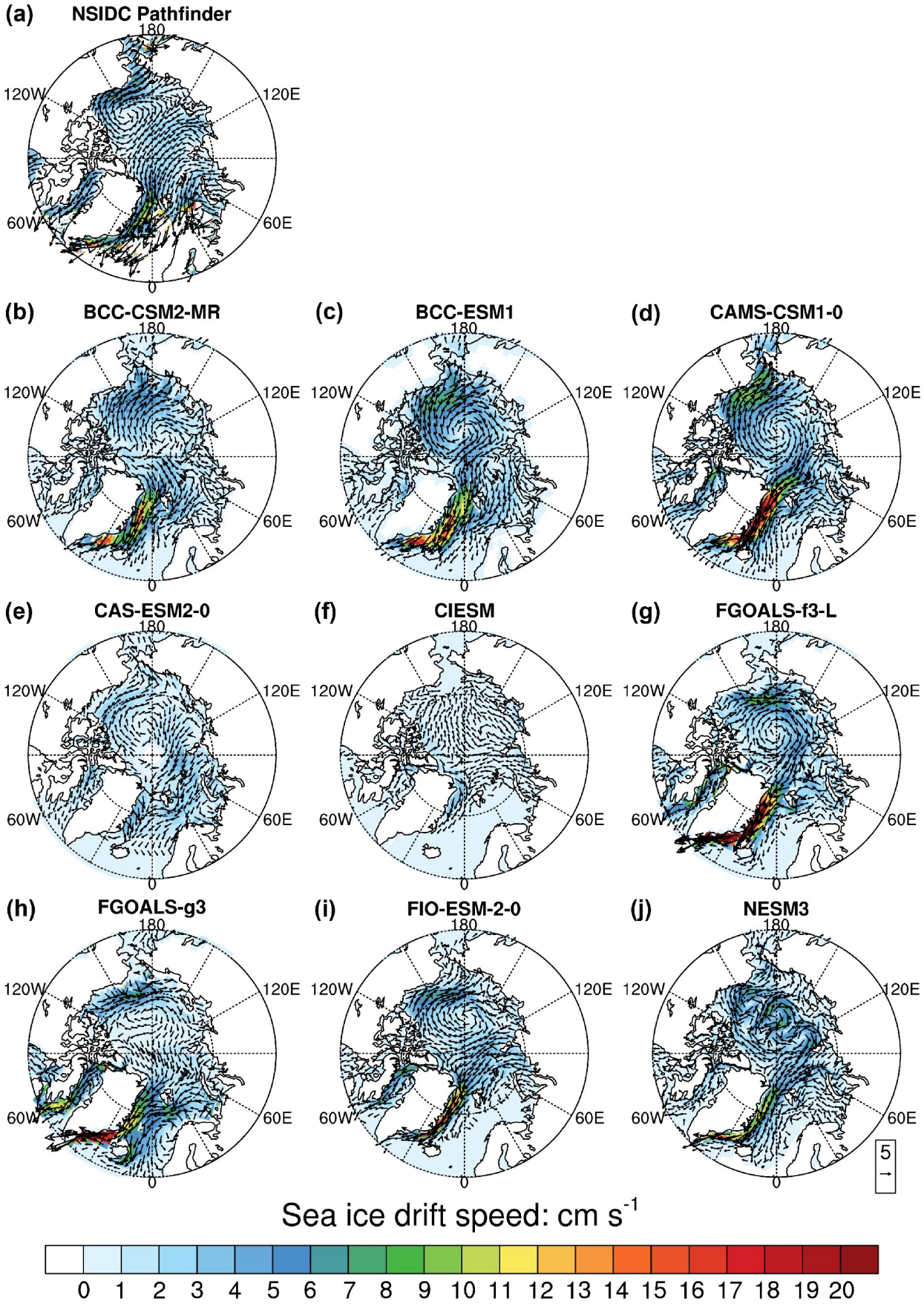

Fig. 2. Same as that in Fig.1, but for autumn (SON).

FGOALS-f3-L, FIO-ESM-2-0, and NESM3) simulate a straight TDS. In CIESM, a reversed TDS is found. For the Arctic sea ice drift pattern shift from spring to autumn, none of the models capture the shrinking of the BG, and only FGOALS-g3 captures the shift of straight a TDS to a curved TDS. Caution is needed when interpreting the NSIDC Pathfinder sea ice drift speed in autumn because large areas of marginal ice zone exist in autumn and the sea ice drift speed uncertainty over the marginal ice zone is large. Previous studies (e.g., Stroeve et al., 2011; Zhang et al., 2021) have shown that the negative phase of Arctic Oscillation (AO) in winter is associated with a stronger BG. Therefore, the BG strength and range differences among the models may be linked to their differences in AO strength and range.

3.2. *Relationship among the spatial patterns of Arctic sea ice drift, near-surface wind, and surface ocean current*

Figures 3a0, b0, and c0 show that the large-scale pattern of the spring sea ice drift over the Arctic in NSIDC Pathfinder is in good agreement with the near-surface wind pattern in ERA-I. Both in the NSIDC Pathfinder sea ice drift and ERA-I near-surface wind, there is an anticyclonic circulation over the Amerasian basin and straight flow from the Siberian coast to the Fram Strait and north of Greenland. In the ORAS4 surface ocean current, however, the extent of the anticyclonic circulation is obviously smaller than that in the sea ice drift field.

Of the nine models, four of them (CAMS-CSM1-0, CIESM, FGOALS-f3-L, and FIO-ESM-2-0) show that the spatial patterns of long-term mean sea ice drift, near-surface wind, and surface ocean current vectors in spring are very similar with each other despite there being some displacements in their anticyclonic centers over the Canadian Basin (Fig. 3). Three of the nine models (BCC-ESM1, BCC-CSM2-MR, and CAS-ESM2-0) also show good agreement between the sea ice drift and near-surface wind patterns, but the agreement between their sea ice drift and surface ocean current patterns is poor. In these two models, the large-scale anticyclonic circulation in sea ice drift is mainly confined in the Amerasian Basin. In contrast, the anticyclonic circulation in surface ocean current almost encloses the whole Arctic Ocean. Two of the nine models (FGOALS-g3 and NESM3) show that the sea ice drift pattern does not match well with the near-surface wind pattern. In FGOALS-g3, a BG appears over the Canadian Basin in the sea ice drift. However, no similar circulation is found over the same area in near-surface wind. Additionally, a cyclonic circulation over the central Arctic appears in near-surface wind while no similar pattern is found in sea ice drift accordingly. In NESM3, the single anticyclonic circulation over the Amerasian Basin in near-surface wind is clearly different from the three small anticyclonic vortices aligned together in the same area in sea ice drift. In contrast, the above sea ice drift pattern in NESM3 matches well with the surface ocean current pattern. Since the corresponding surface ocean current magnitude is much larger than the sea ice drift magnitude, the distinct sea ice drift pattern over the Amerasian Basin in NESM3 is likely driven by the surface ocean current.

Figure 4 shows that although the sea ice drift, near-surface wind, and surface ocean current patterns in autumn (September-October-November; SON) are different from those in spring in the observation/reanalysis, the spatial pattern among these three variables is very similar. The pattern agreement among the sea ice drift, near-surface wind, and surface ocean current in autumn is also very similar to that in spring in each model except for CIESM. In CIESM, the sea ice drift pattern in autumn is no longer in good agreement with the near-surface wind and surface ocean current patterns.

3.3. *Relationship among the trend patterns of Arctic sea ice drift, surface ocean current, near-surface wind*

The trends in spring sea ice drift, near-surface wind, and surface ocean current magnitude (indicated by the color shadings) and their vector components (indicated by the arrows) are shown in Fig. 5. The latter shows the direction of the change in sea ice drift, near-surface wind, and surface ocean current. The areas that the confidence level of the magnitude trend is less than 95% are masked out. The spring sea ice drift speed significantly increased over most of the Arctic during 1979–2014 in the NSIDC Pathfinder (Fig. 5a0). This is consistent with the trend found in Zhang et al. (2021), which also calculated based on NSIDC Pathfinder. The trend vector (indicated by the arrows) also shows that both the BG and TDS are enhanced in the NSIDC Pathfinder (For BG, the trend is about 0.8–1.2 cm s^{-1} $(10\ yr)^{-1}$ near Alaska/Canada coast; for TDS, the trend is about 1.6–2.0 cm s^{-1} $(10\ yr)^{-1}$ near the Fram Strait). These observational sea ice drift speed increases seem not to be wind-driven because no significant near-surface wind speed changes are found over the corresponding areas in ERA-I. Only a small area of sea ice drift speed decrease over the Siberian coast is matched with the decrease of near-surface wind speed (Fig. 5b0). The observed sea ice drift speed increases are, at most, weakly link to surface ocean current speed changes because the surface ocean current speed in ORSA4 only changes significantly over some narrow, band-shaped areas over the Arctic (Fig. 5c0). Therefore, the observed Arctic sea ice drift acceleration during 1979–2014 is more likely caused by the increased response of the sea ice drift to the wind. This is supported by the fact that the wind factor (the sea ice drift speed from NSIDC Pathfinder divided by the near-surface wind speed from ERA-I) in the observation/reanalysis increases significantly over the sea ice drift speed acceleration areas (Fig. S1 in the electronic supplementary material).

There are three models (FGOALS-f3-L, FGOALS-g3, and NESM3) that partly capture the spring sea ice drift speed acceleration over the Arctic (Fig. 5). In FGOALS-f3-L, the significant sea ice drift speed increase only appears

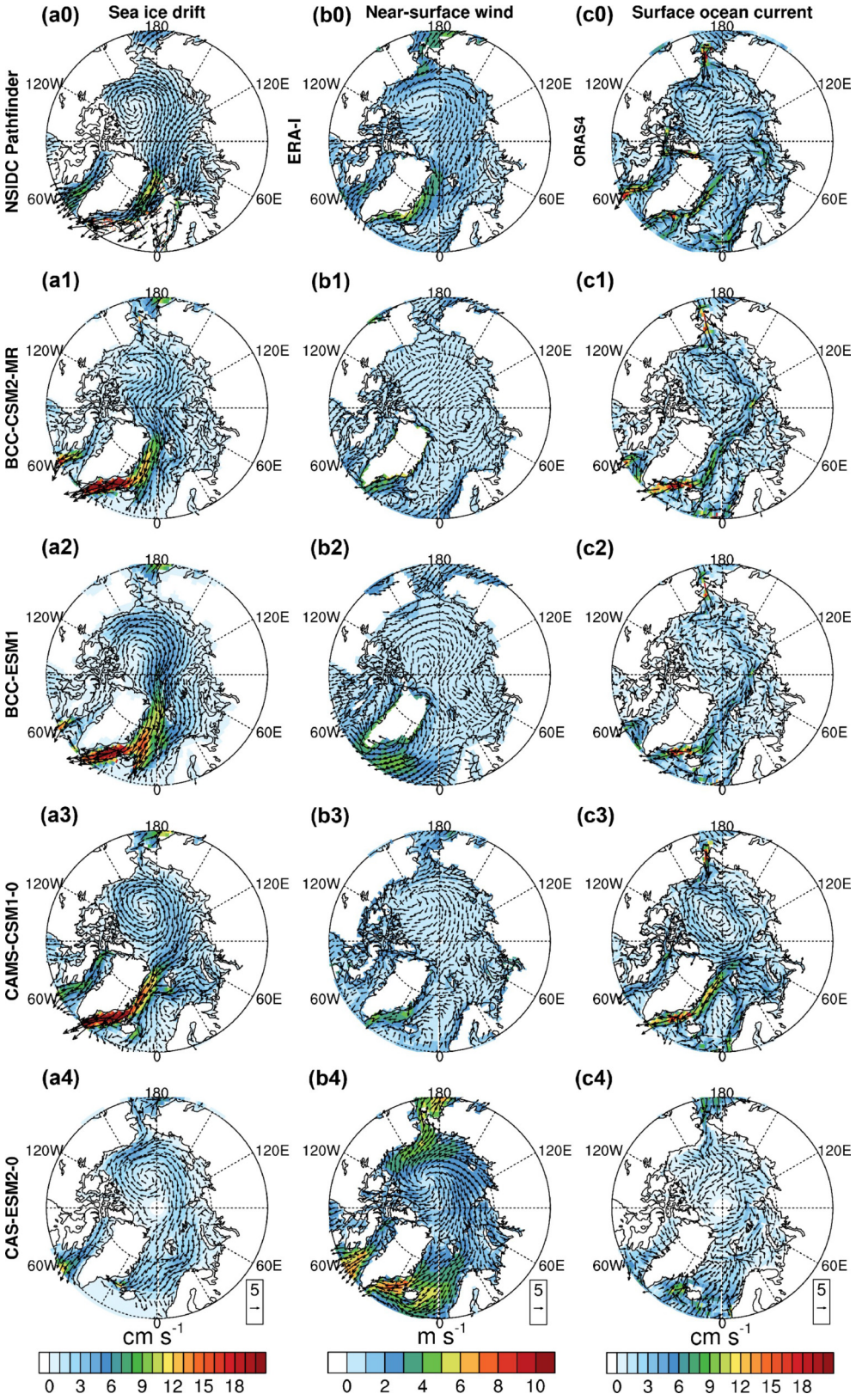

Fig. 3. Spatial pattern of the spring (MAM) long-term (1979–2014) mean direction (vector) and speed (shading) of sea ice drift (left), near-surface wind (middle), and surface ocean current (right) in the observation/reanalysis (NSIDC Polar Pathfinder for sea ice drift, ERA-Interim for near-surface wind, and ORAS4 for upper layer ocean current) and nine CMIP6 models (BCC-CSM2-MR, BCC-ESM1, CAMS-CSM1-0, CAS-ESM2-0, CIESM, FGOALS-f3-L, FGOALS-g3, FIO-ESM-2-0, and NESM3) from China.

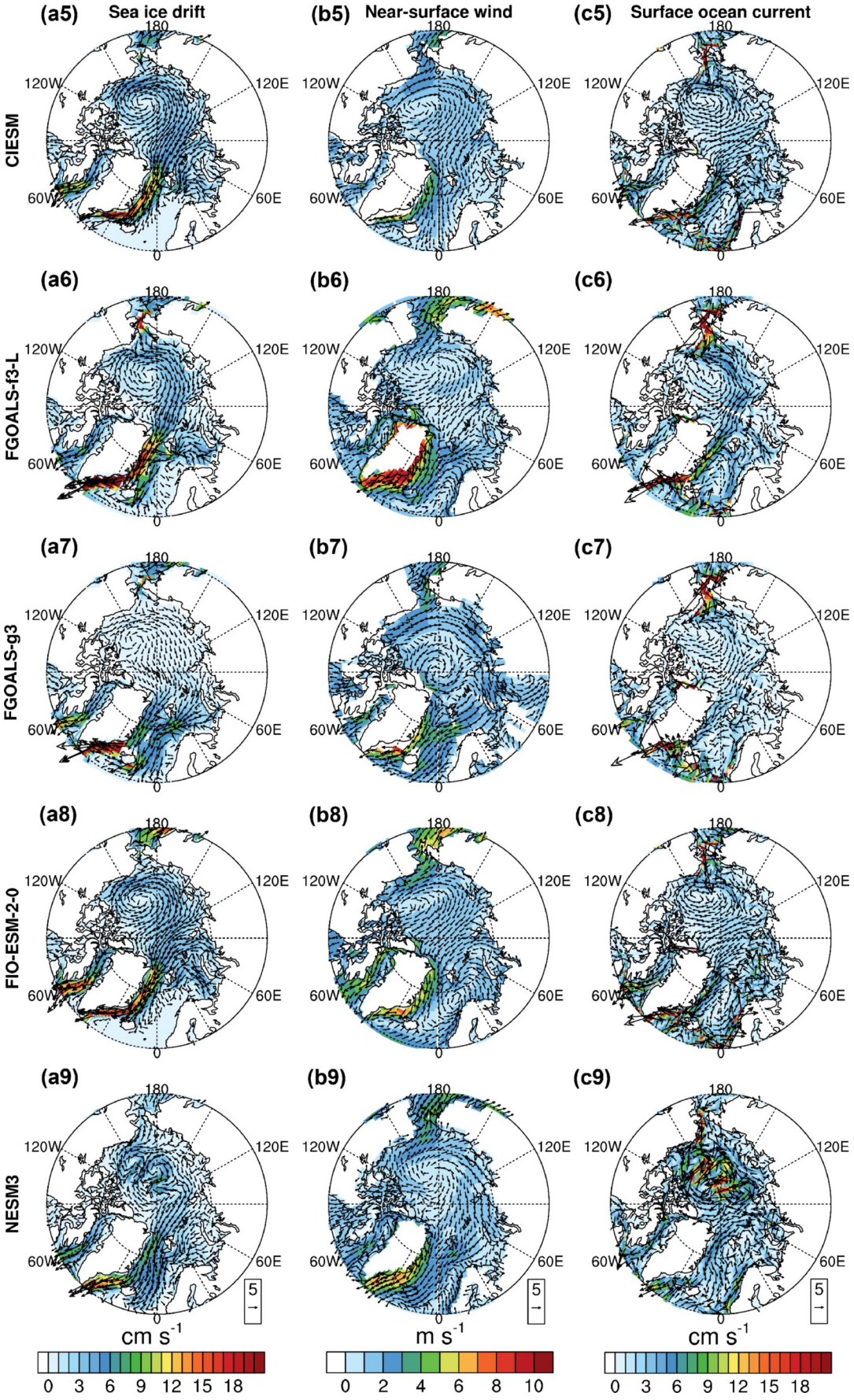

Fig. 3. (Continued).

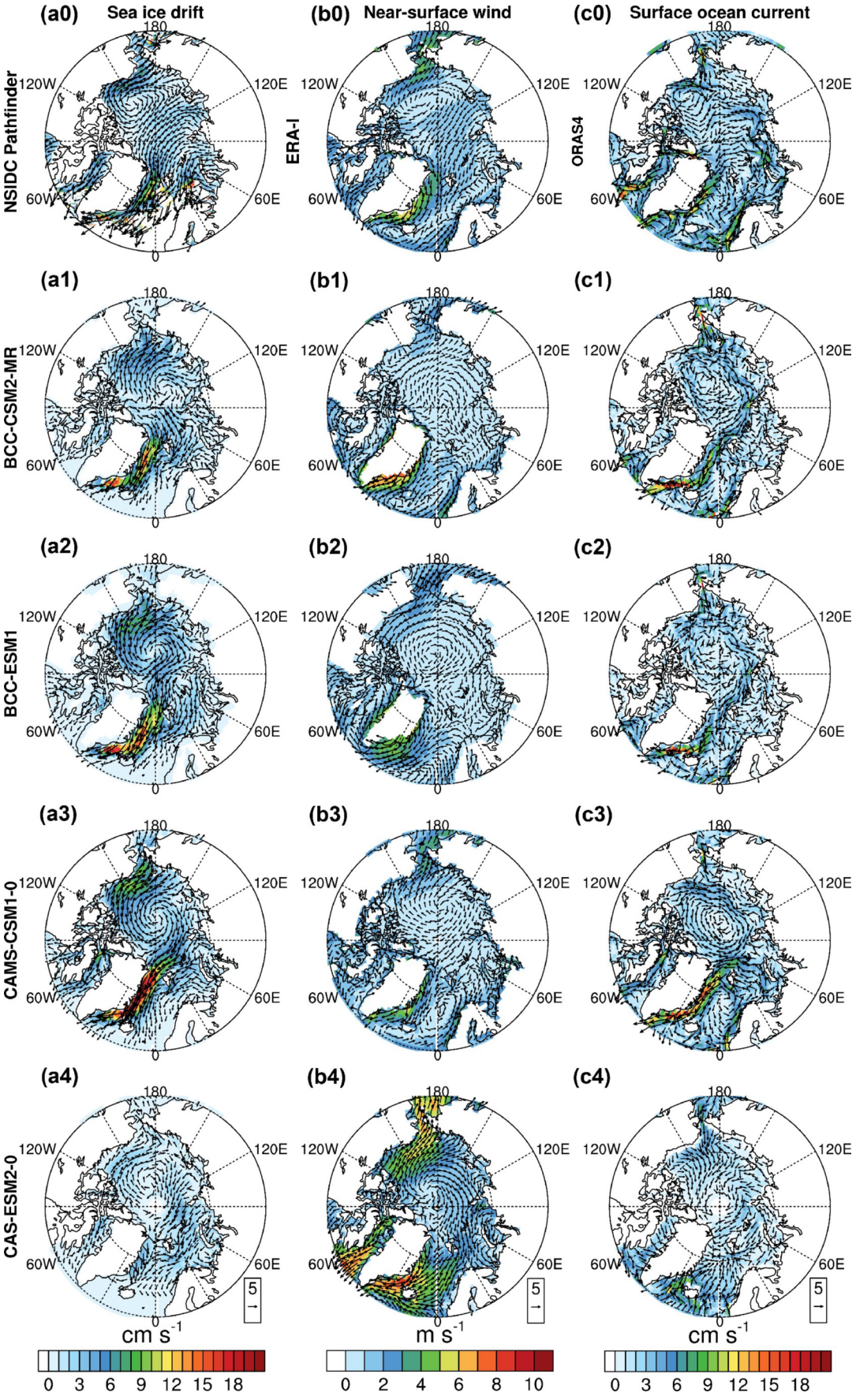

Fig. 4. Same as that in Fig. 3, but for autumn (SON).

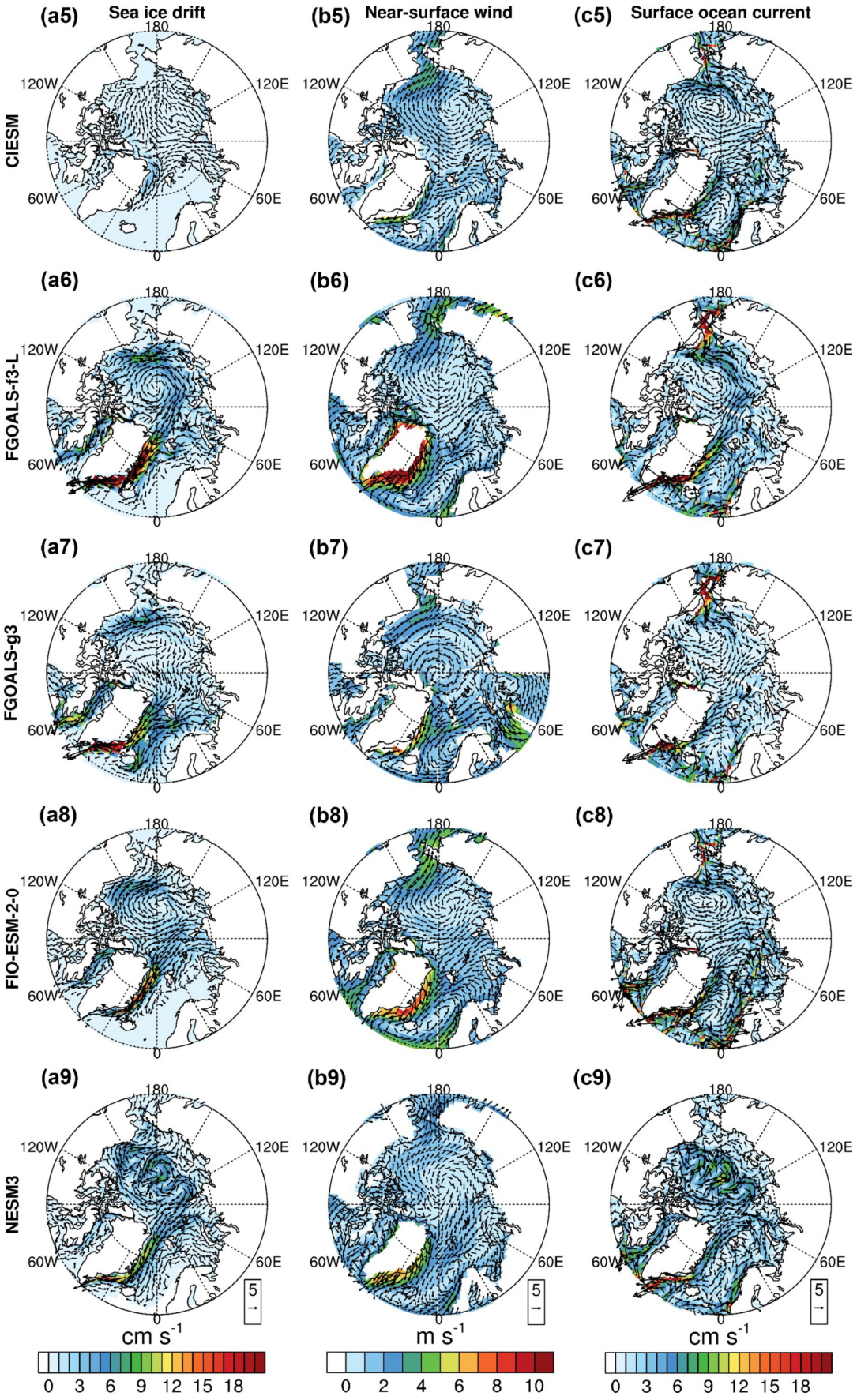

Fig. 4. (Continued).

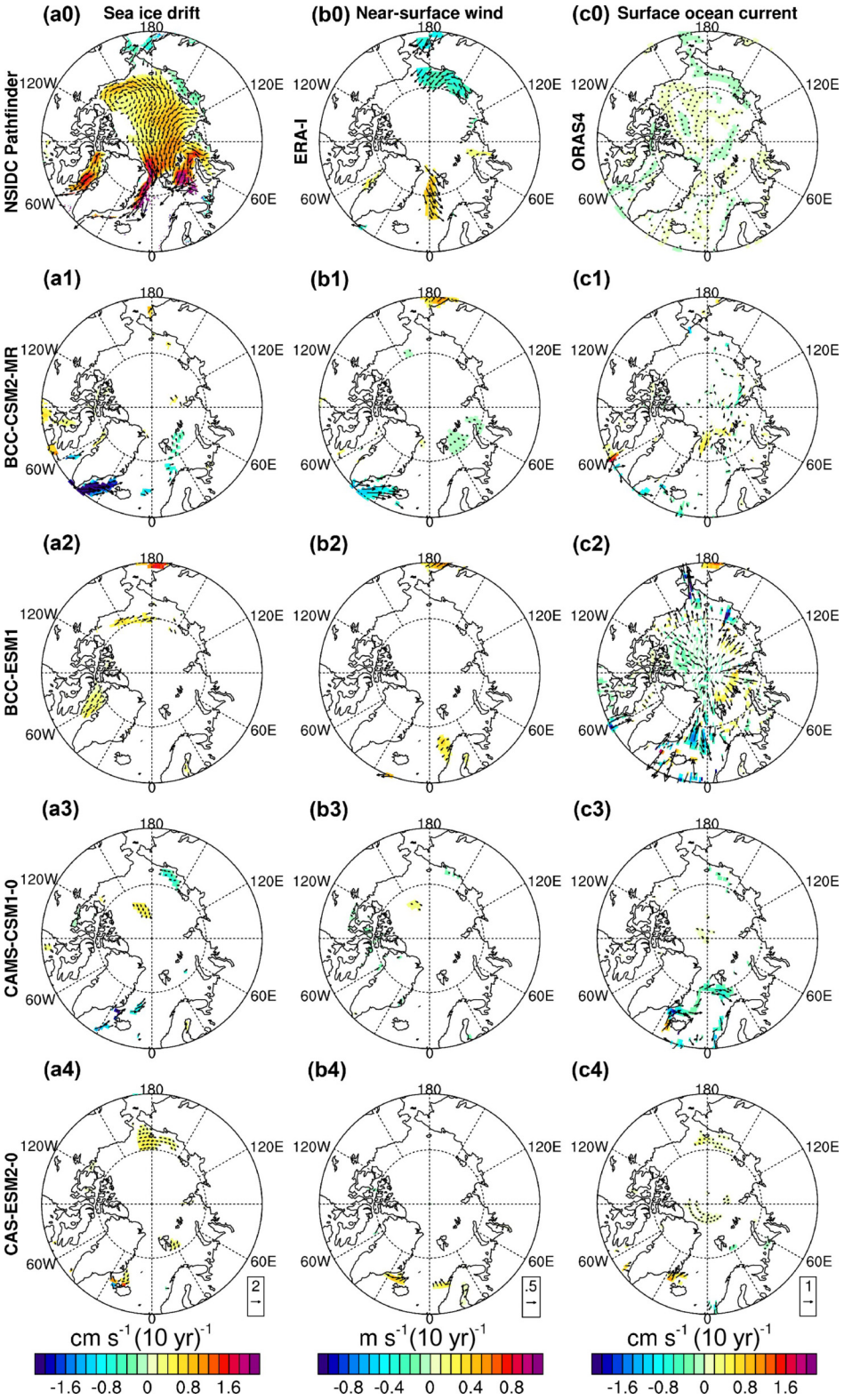

Fig. 5. The trend of spring (MAM) sea ice drift (left), near-surface wind (middle), and surface ocean current (right) in the observation/reanalysis (NSIDC Polar Pathfinder for sea ice drift speed, ERA-Interim for near-surface wind speed, and ORAS4 for upper layer ocean current) and nine CMIP6 models (BCC-CSM2-MR, BCC-ESM1, CAMS-CSM1-0, CAS-ESM2-0, CIESM, FGOALS-f3-L, FGOALS-g3, FIO-ESM-2-0, and NESM3) from China for the period of 1979–2014. Colors and arrows represent the trend in the magnitude and vector components of sea ice drift, near-surface wind, and surface ocean current, respectively. Areas where the confidence level of the magnitude trend is less than 95% are masked out.

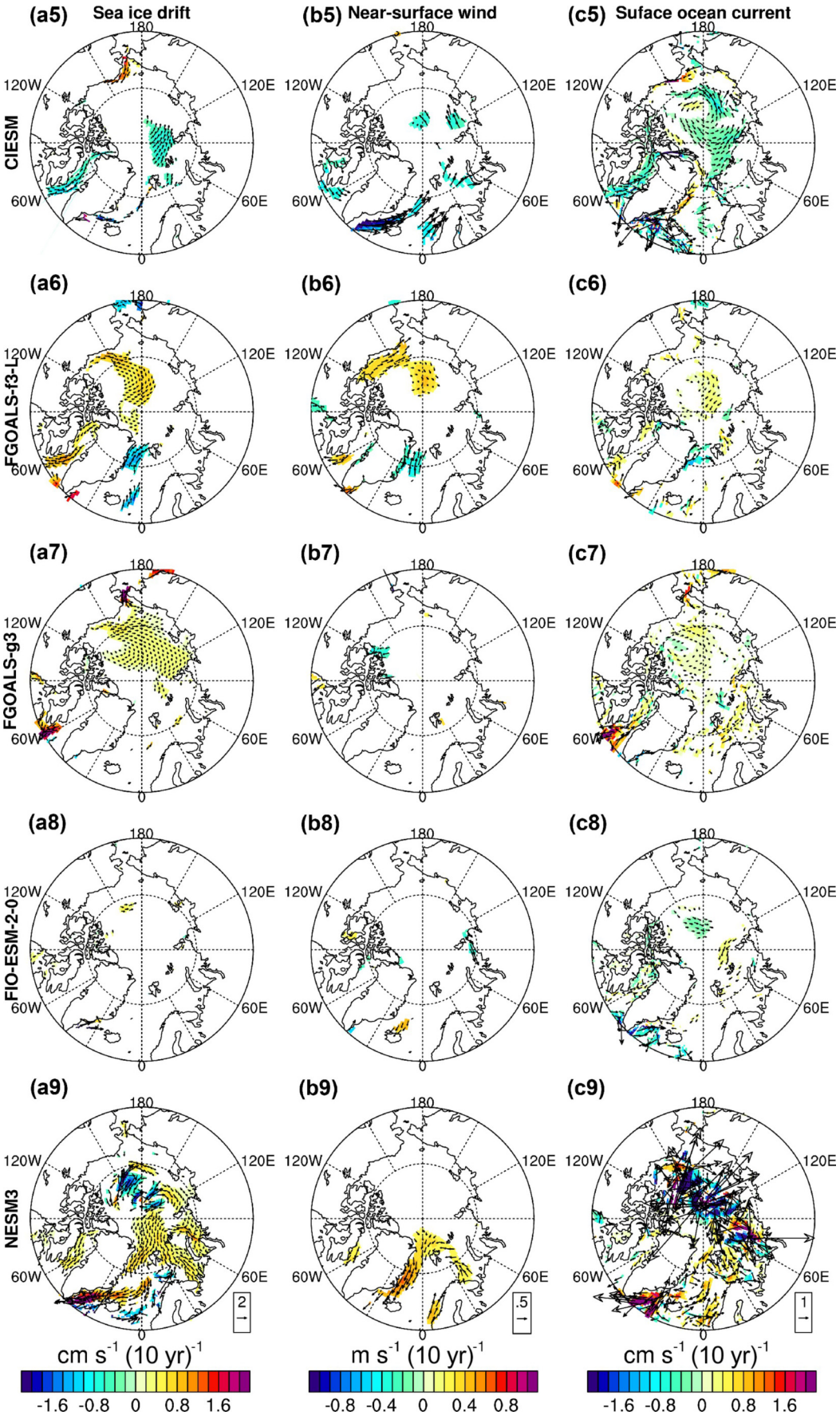

Fig. 5. (Continued).

over the north of the Beaufort Sea, part of the central Arctic, the Baffin Bay, and the Davis Strait (Fig. 5a6). These changes may be driven by the wind speed acceleration because significant near-surface wind speed increases are associated with them. The sea ice drift speed increases over the central Arctic are also associated with the surface ocean current speed increases. In FGOALS-g3, the significant sea ice drift speed increase appears approximately over the area between 120°W and 110°E (Fig. 5a7). These increases are unlikely to be wind-driven because no significant near-surface wind speed changes are associated with them. Over the north of the Beaufort Sea, however, there are significant surface ocean current speed increases associated with the sea ice drift speed increases. In NESM3, the significant sea ice drift speed increases appear mainly over the Laptev Sea, Kara Sea, Barents Sea, Fram Strait, and part of the central Arctic (Fig. 5a9). These changes are not wind-driven except over the north and south of the Fram Strait and the west of the Barents Sea, where significant near-surface wind speed increases appear. Additionally, there are some areas of significant sea ice drift speed decreases over the Canadian Basin in NESM3, and they are associated with the strong significant surface ocean current speed decreases over the same area. In the other six models (BCC-CSM2-MR, BCC-ESM1, CAMS-CSM1-0, CAS-ESM2-0, CIESM, and FIO-ESM-2-0), there are only a few scattered areas of significant sea ice drift speed, near-surface wind speed, and surface ocean current speed changes, and their locations are not matched well (Fig. 5).

In autumn, the sea ice drift trends and their relationship with the near-surface wind speed and surface ocean current speed trends in the observation/reanalysis data (Figs. 6a0, b0, and c0) are similar to those in spring in the following way: the autumn sea ice drift speed also increases significantly over most of the Arctic, and the BG and TDS are also strengthened during 1979–2014 in the NSIDC Pathfinder. The sea ice drift speed trends in autumn are also not wind-driven because no significant near-surface wind speed trends in ERA-I are associated with them. They are only weakly linked with the surface ocean current speed trends. The differences between the autumn and spring sea ice drift trends are in their magnitudes and patterns. The autumn sea ice drift speed trends over the southern Canadian Basin and the Chukchi Sea are much larger than those in spring. The autumn sea ice drift trend vectors over the north of the Laptev Sea are more curved than those in spring.

Compared to the observation/reanalysis, the autumn sea ice drift speed trends in the nine models are only significant over a small part of the Arctic (Fig. 6). These areas are almost only located outside the central Arctic except in NESM3, in which significant sea ice drift speed trends appear over a few narrow band-shaped areas in the central Arctic. Areas with significant near-surface wind speed and surface ocean current speed trends are also small, and they are rarely co-located with the significant sea ice drift speed trends in the nine models.

4. Arctic basin-wide mean sea ice drift speed, near-surface wind speed, and surface ocean current speed

4.1. *Climatology of Arctic basin-wide mean sea ice drift speed*

Figure 7 shows that both the simulated magnitude and seasonal evolution of the Arctic basin-wide (the domain is defined by the SCICEX box, which is shown as the red box in Fig. 1a) mean sea ice drift speed vary among the nine models and are different from those in the observation. In NSIDC Pathfinder, the monthly Arctic sea ice drift speed climatology (1979–2014) varies from 2.36 cm s^{-1} (in July) to 4.14 cm s^{-1} (in October) across different months. The ensemble means of the sea ice drift speed from the nine models are overestimated in all the months. Individually, five of the nine models (BCC-CSM2-MR, BCC-ESM1, CAMS-CSM1-0, FGOALS-f3-L, and FIO-ESM-2-0) overestimate the climatological sea ice drift speed for all the months. One model (FGOALS-g3) underestimates the sea ice drift speed for all the months. CAS-ESM2-0 overestimates the sea ice drift speed from July to September and underestimates the sea ice drift speed in the other months. NESM3 overestimates the sea ice drift speed from March to October, especially in July (overestimated by 3.38 cm s^{-1}), and underestimates the sea ice drift speed in the other months. CIESM overestimates the sea ice drift speed from December to July and underestimates the sea ice drift speed in the other months. The climatological sea ice drift speed in CIESM is very low from August to October. The September sea ice drift speed is near zero.

The seasonality of the sea ice drift speed in the model ensemble mean is similar to that in the NSIDC Pathfinder. Individually, however, none of the models reach a minimum in July like the observation does: four reach a minimum in May, two in September, one in January, one in February, and one in August. The simulated sea ice drift speed from three of the models even peaks in July. Another three models peak in October (same with the observation), one in November, one in December, and one in January. The seasonal variability among the 12 months (defined as the standard deviation of the climatological sea ice drift speed in 12 months) is 0.53 cm s^{-1} in the NSIDC Pathfinder. In the nine models, the sea ice drift speed seasonal variabilities in BCC-CSM2-MR (0.54 cm s^{-1}), CAMS-CSM1-0 (0.57 cm s^{-1}), and FGOALS-g3 (0.50 cm s^{-1}) are close to that in the NSIDC Pathfinder. The variabilities in BCC-ESM1 (0.84 cm s^{-1}), CAS-ESM2-0 (0.71 cm s^{-1}), CIESM (2.21 cm s^{-1}), FIO-ESM-2-0 (0.81 cm s^{-1}), and NESM3 (1.29 cm s^{-1}) are obviously larger than that in the NSIDC Pathfinder. In particular, the sea ice drift speed seasonal variabilities in CIESM and NESM3 are about 2.4 and 4.2 times that in the NSIDC Pathfinder, respectively. The variability in FGOAL-f3-L (0.34 cm s^{-1}) is smaller than that in the NSIDC Pathfinder.

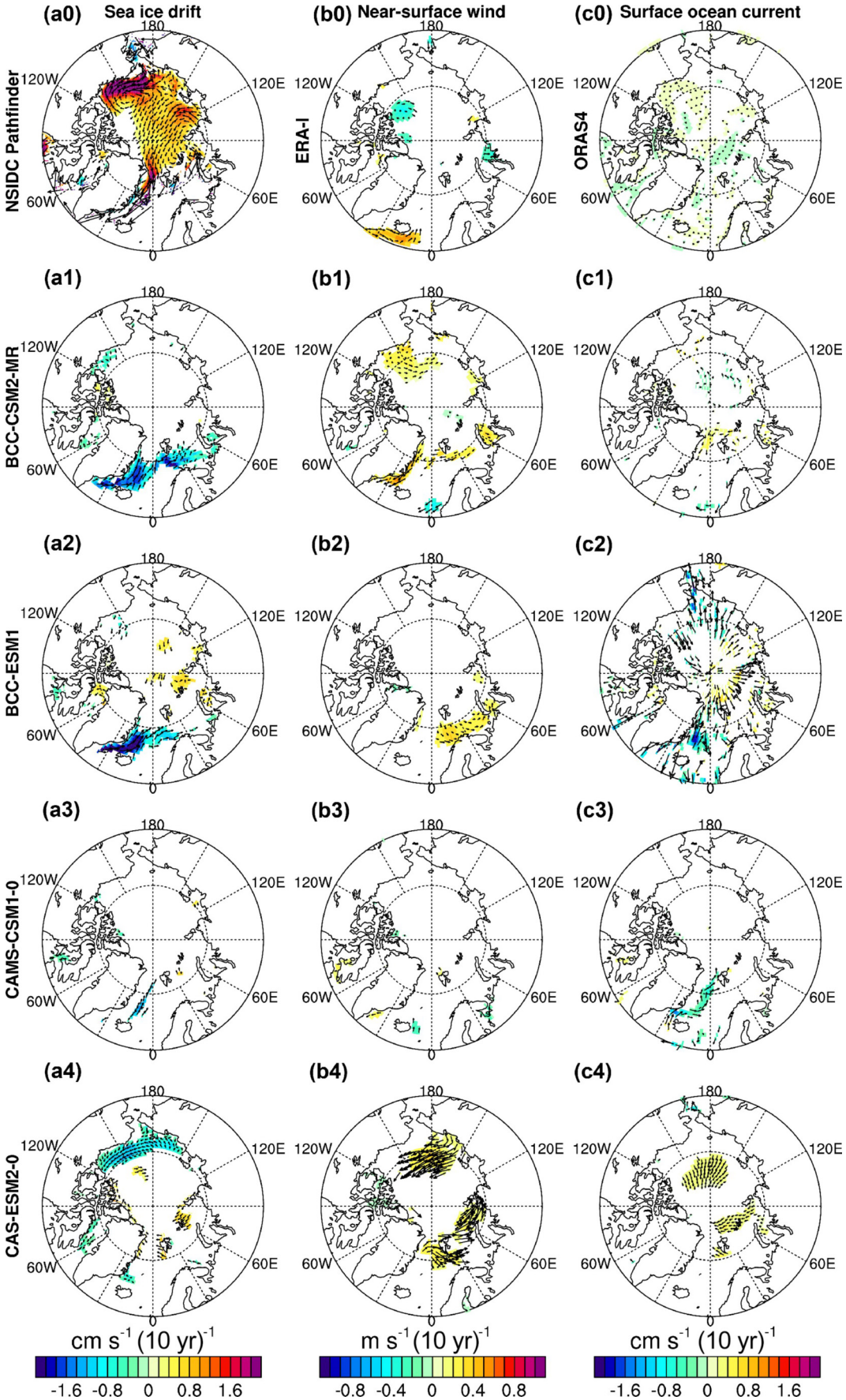

Fig. 6. Same as that in Fig. 5, but for autumn (SON).

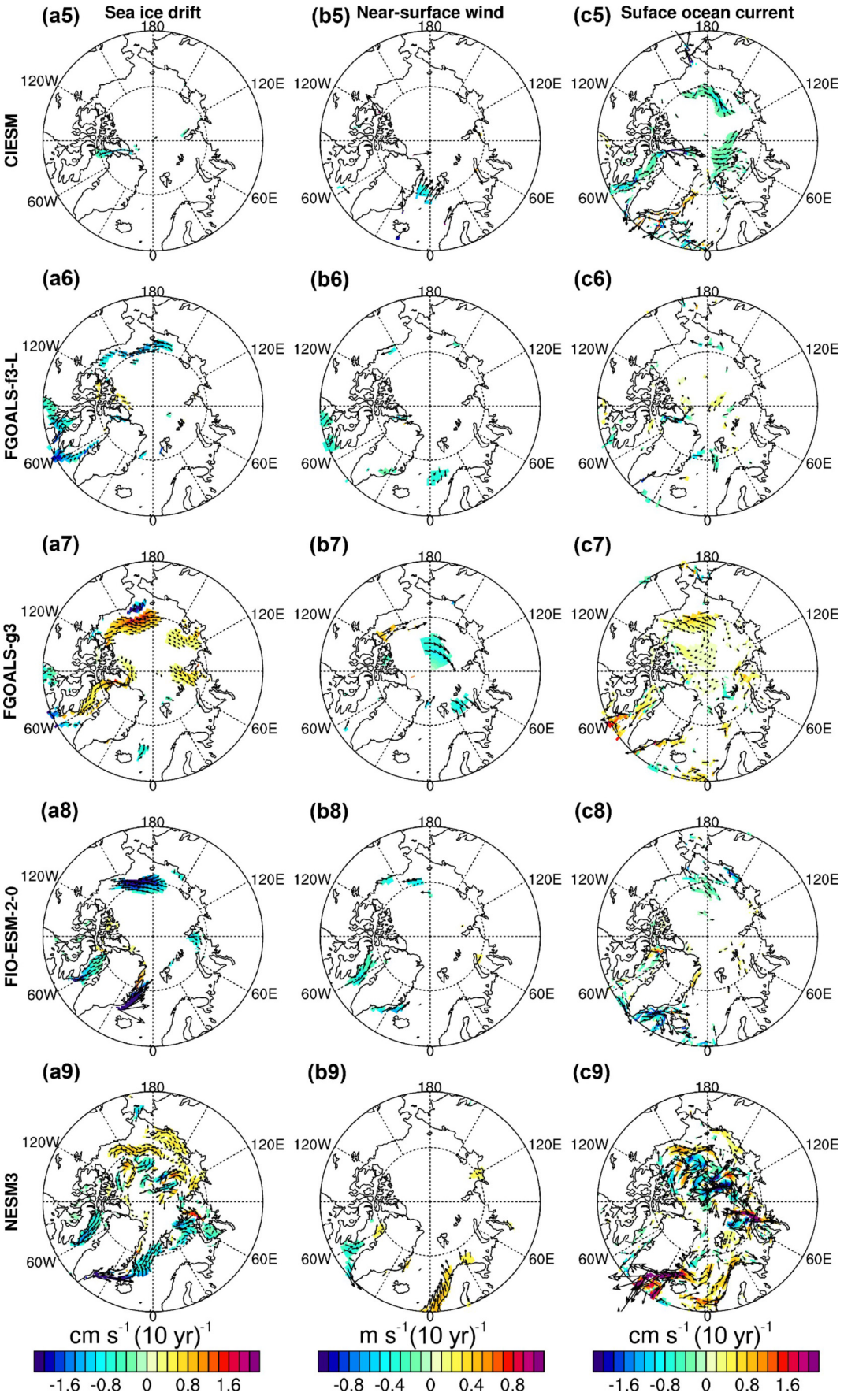

Fig. 6. (Continued).

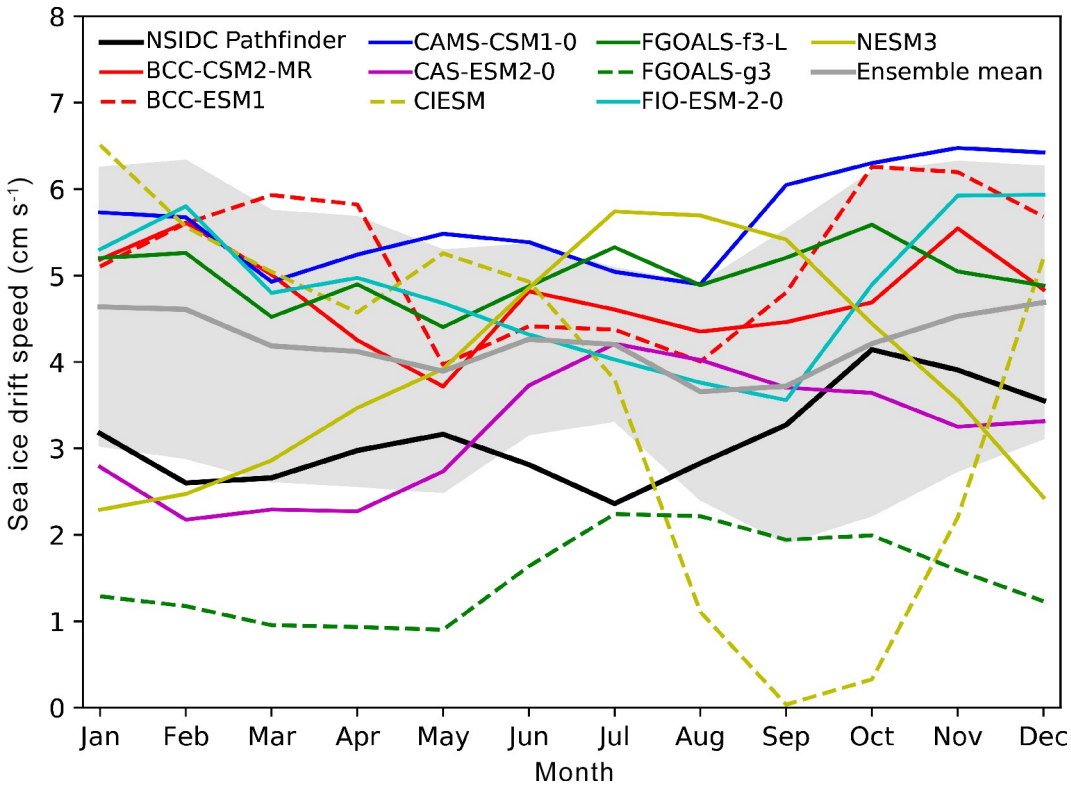

Fig. 7. Arctic basin-wide mean sea ice drift speed (cm s^{-1}) in NSIDC Polar Pathfinder (black line) and nine CMIP6 models (BCC-CSM2-MR, BCC-ESM1, CAMS-CSM1-0, CAS-ESM2-0, CIESM, FGOALS-f3-L, FGOALS-g3, FIO-ESM-2-0, and NESM3) from China for the period of 1979–2014. The domain of the spatial mean is the same as the SCICEX domain, which is marked as the red box in Fig. 1a.

In order to understand which range of sea ice drift speed was the main cause of the bias in the Arctic mean sea ice drift speed in these nine models, we present the probability distribution of the Arctic sea ice drift in the models against that in the NSIDC Pathfinder (Figs. 8 and 9). Figure 8 shows that six models (BCC-CSM2-MR, BCC-ESM1, CAMS-CSM1-0, CIESM, FGOALS-f3-L, and FIO-ESM-2-0) overestimate the mean sea ice drift speed in MAM because they overestimate the frequency of the high-speed component and underestimate the frequency of the low-speed component. The threshold between the overestimation and underestimation for these models ranges from 3.2 cm s^{-1} (BCC-CSM2-MR) to 4.0 cm s^{-1} (BCC-ESM1). The MAM sea ice drift speed distribution in NESM3 is close to the observation, with a slight overestimation of sea ice drift speed between 2.0 cm s^{-1} and 4.9 cm s^{-1}. Two models (CAS-ESM2-0 and FGOALS-g3) underestimate the mean sea ice drift speed because they overestimate the frequency of the low-speed component and underestimate the frequency of the high-speed component. The threshold between the overestimation and underestimation for CAS-ESM2-0 and FGOALS-g3 is 2.6 cm s^{-1} and 1.7 cm s^{-1}, respectively.

In SON, seven models (BCC-CSM2-MR, BCC-ESM1, CAMS-CSM1-0, CAS-ESM2-0, FGOALS-f3-L, FIO-ESM-2-0, and NESM3) overestimate the mean sea ice drift speed because they overestimate the frequency of the high-speed component and underestimate the frequency of the low-speed component (Fig. 9). The threshold between the overestimation and underestimation for these models ranges from 3.0 cm s^{-1} (CAS-ESM2-0) to 4.4 cm s^{-1} (CAMS-CSM1-0). Two models (CIESM and FGOALS-g3) underestimate the mean sea ice drift speed because they overestimate the frequency of the low-speed component and underestimate the frequency of the high-speed component. The threshold between the overestimation and underestimation for CIESM and FGOALS-g3 is 2.4 cm s^{-1} and 2.3 cm s^{-1}, respectively.

4.2. *Relationship among the climatology of Arctic basin-wide mean sea ice drift speed, surface ocean current speed, and near-surface wind speed*

The seasonal evolution of the Arctic basin-wide mean sea ice drift speed, surface ocean current speed, and near-surface wind speed are shown in Fig. 10. There is no clear relation between the seasonal variations of the sea ice drift speed and near-surface wind speed in the observation/reanalysis data. In contrast, the seasonal variation of the sea ice drift speed agrees with that of the surface ocean current speed. Also, the seasonal variation of the near-surface wind speed agrees with that of the surface ocean current speed.

Three of the models (CAS-ESM2-0, CIESM, and FGOALS-f3-L) agree with the observation/reanalysis in that there is no clear agreement between the seasonal variation of the Arctic basin-wide mean sea ice drift speed and

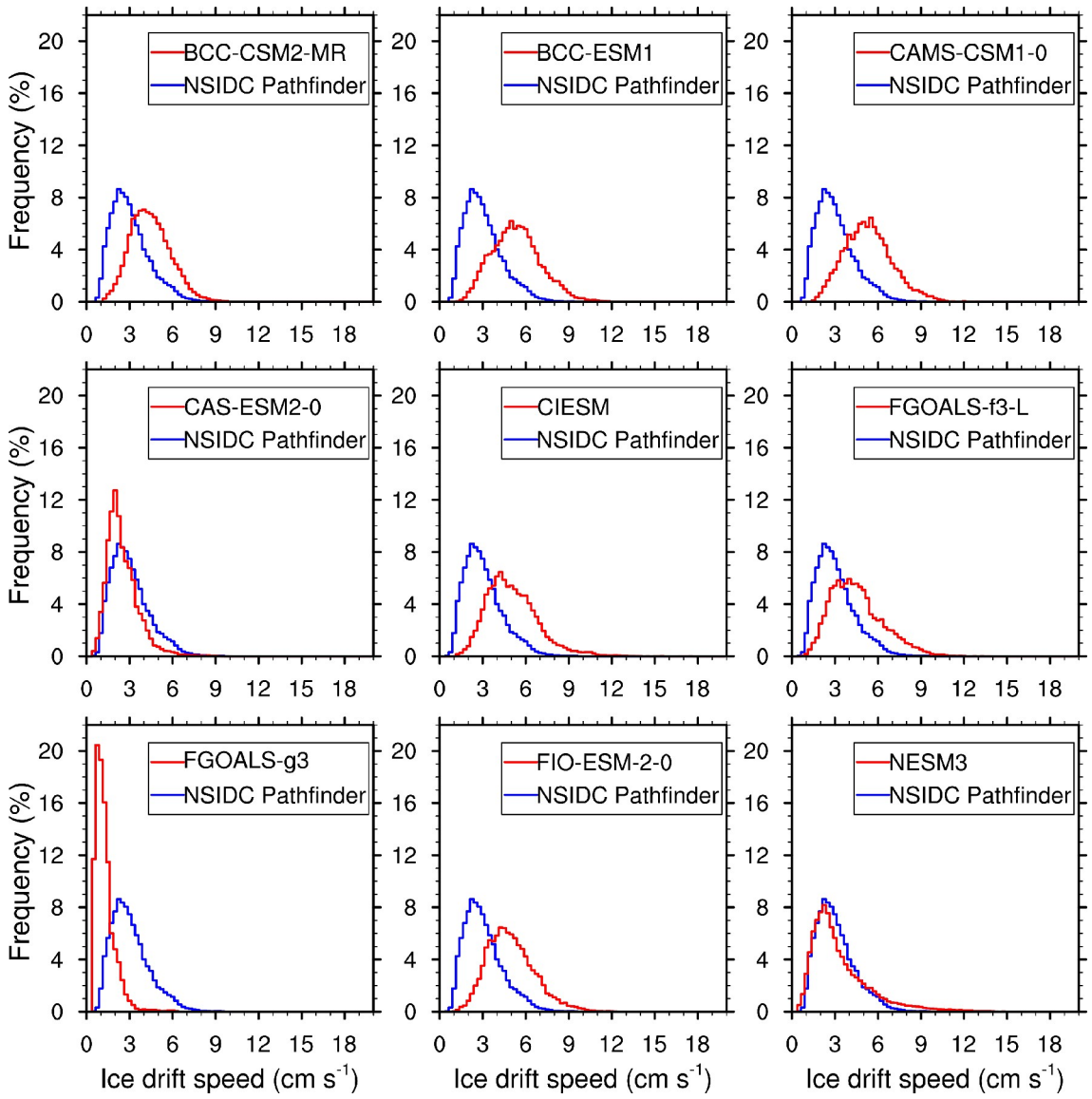

Fig. 8. The frequency distribution of the spring (MAM) Arctic sea ice drift speed in nine CMIP6 models (BCC-CSM2-MR, BCC-ESM1, CAMS-CSM1-0, CAS-ESM2-0, CIESM, FGOALS-f3-L, FGOALS-g3, FIO-ESM-2-0, and NESM3) for the period of 1979–2014 against that in the NSIDC Polar Pathfinder (blue line). The domain of probability distribution calculation is the same as the SCICEX domain, which is marked as the red box in Fig. 1a.

near-surface wind speed. Of the remaining six models, four of them (BCC-CMS2-MR, BCC-ESM1, CAMS-CSM1-0, and FIO-ESM-2-0) show that the sea ice drift speed and the near-surface wind speed are in agreement with each other. Two of them (FGOALS-g3 and NESM3) show that the sea ice drift speed and the near-surface wind speed are negatively correlated. For the relation between the seasonal variation of the sea ice drift speed and surface ocean current speed, four of the models (BCC-CMS2-MR, BCC-ESM1, CAMS-CSM1-0, and FIO-ESM-2-0) show good agreement. There is no clear agreement in the remaining five models (CAS-ESM2-0, CIESM, FGOALS-f3-F, GOALS-g3, and NESM3). The agreement between the near-surface wind speed and surface ocean current speed is good in two of the models (BCC-CMS2-MR and BCC-ESM1). The remaining seven models show no clear agreement between the near-surface wind speed and surface ocean current speed.

4.3. *Trend of Arctic basin-wide mean sea ice drift speed*

Figures 11 and 12 show the time series and linear trends of the Artic basin-wide mean sea ice drift speed in spring and autumn, respectively, during 1979–2014. In the observation, the spring Arctic sea ice drift speed increases significantly with a rate of 0.64 cm s^{-1} (10 yr)$^{-1}$ from 1979 to 2014 (Fig. 11). In the models, however, only FGOALS-g3 shows a significant increase in spring Arctic sea ice drift speed, and the trend is much weaker [0.18 cm s^{-1} (10 yr)$^{-1}$]. NESM3 shows a weak and significant decrease [–0.15 cm s^{-1} (10 yr)$^{-1}$] in the Arctic sea ice drift speed. For the other seven models, no significant trend in the Arctic sea ice drift

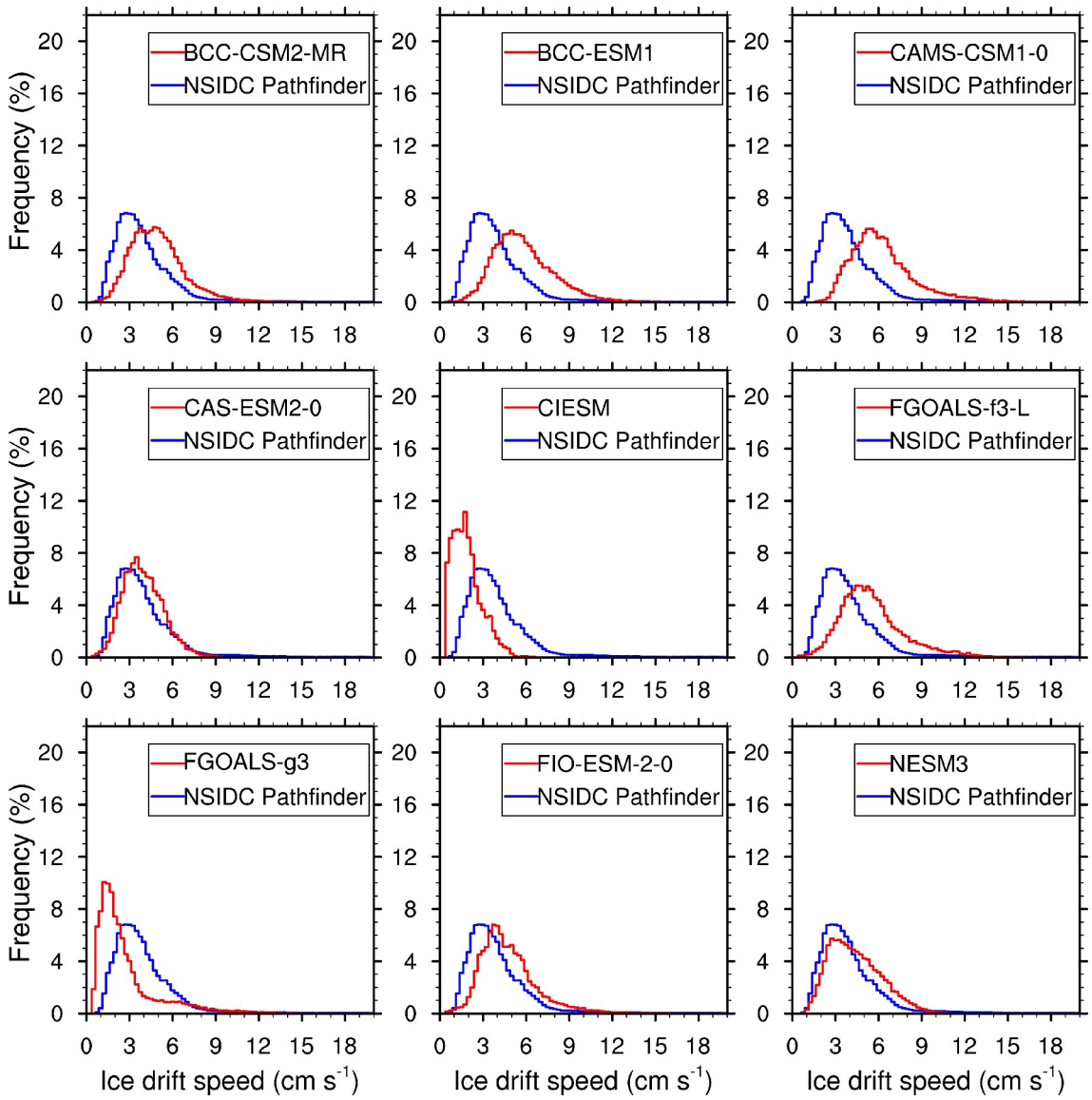

Fig. 9. Same as that in Fig. 8, but for autumn (SON).

speed is detected. In autumn, the observational Arctic sea ice drift speed shows a significant increase with a rate of 0.89 cm s^{-1} $(10\ yr)^{-1}$ from 1979 to 2014 (Fig. 12), which is larger than that in spring. Of the models, also only FGOALS-g3 shows a significant Arctic sea ice drift speed increase, with a rate of 0.12 cm s^{-1} $(10\ yr)^{-1}$. No significant Arctic sea ice drift speed trend is found for the other eight models. Zhang et al. (2021) also investigated the linear trends of the Arctic basin-wide mean sea ice drift speed based on the NSIDC Pathfinder product and shows larger trends in spring and autumn than those found in this study. This may be linked to the differences in spatial average domain and time period between our study and Zhang et al. (2021).

5. Summary and conclusions

We have evaluated the Arctic sea ice drift and its relationship with the near-surface wind and surface ocean current in the historical runs of nine CMIP6 models from China. These models are BCC-CSM2-MR, BCC-ESM1, CAMS-CSM1-0, CAS-ESM2-0, CIESM, FGOALS-f3-L, FGOALS-g3, FIO-ESM-2-0, and NESM3. Sea ice drift from the NSIDC Pathfinder product, near-surface wind from ERA-I, and surface ocean current from ORAS4 are used to evaluate the model results for the period of 1979–2014. Both the spatial patterns and the Arctic basin-wide mean (averaged over the SCICEX domain) of the sea ice drift, near-surface wind, and surface ocean current are compared. The main conclusions are listed below:

(1) All nine models capture the Beaufort Gyre (BG) and the Transpolar Drift Stream (TDS) in spring except for NESM3, in which there are three small anticyclonic vortices aligned together instead of a BG over the Amerasian basin. These anticyclonic vortices are likely current-driven. Four of the nine models show similar extent, location, and

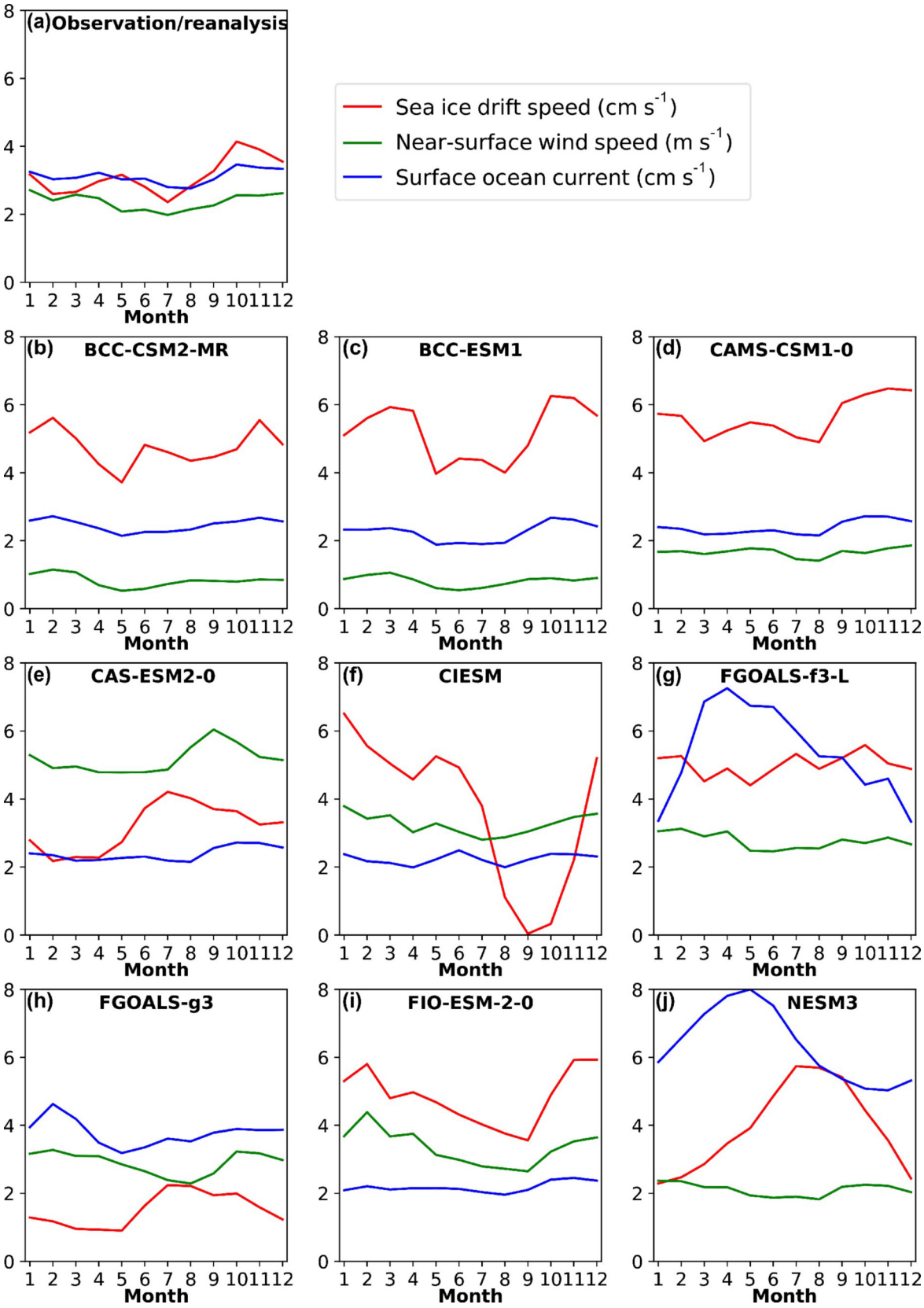

Fig. 10. The seasonal cycle of Arctic basin-wide mean sea ice drift speed (cm s^{-1}, red line), near-surface wind speed (m s^{-1}, green line), and surface ocean current (cm s^{-1}, blue line) in the observation/reanalysis (NSIDC Polar Pathfinder for sea ice drift speed, ERA-Interim for near-surface wind speed, and ORAS4 for upper layer ocean current) and in nine CMIP6 models from China for the period of 1979–2014. The domain of the spatial mean is the same as the SCICEX domain, which is marked as the red box in Fig. 1a.

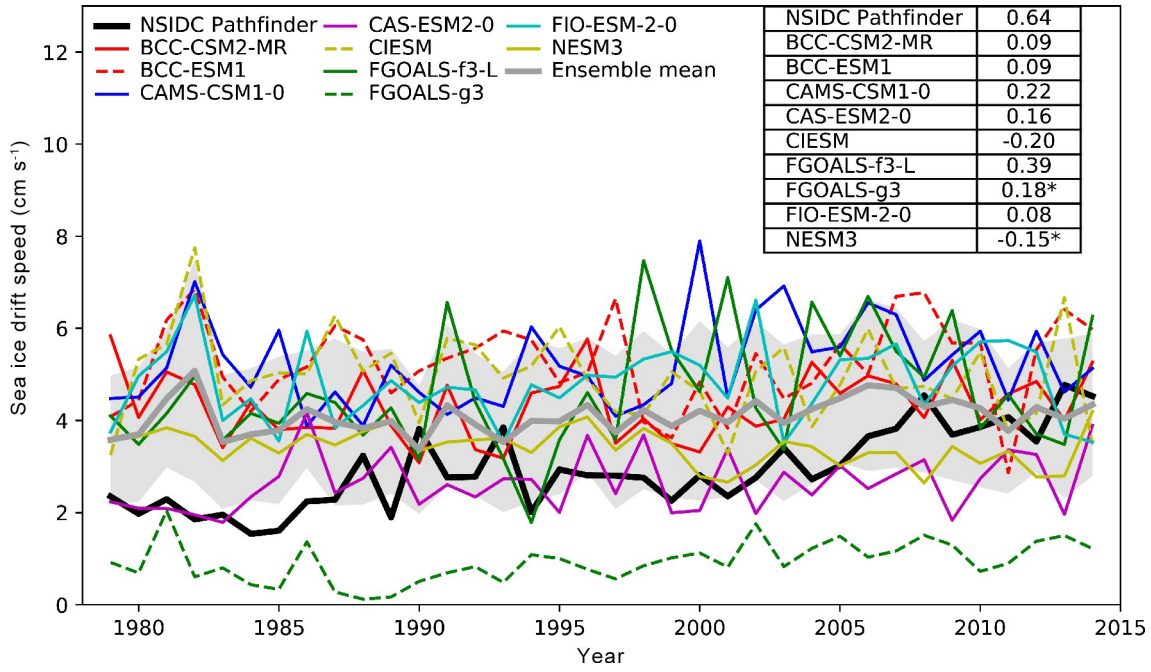

Fig. 11. Arctic mean spring (MAM) sea ice drift speed in NSIDC Polar Pathfinder and nine CMIP6 models (BCC-CSM2-MR, BCC-ESM1, CAMS-CSM1-0, CAS-ESM2-0, CIESM, FGOALS-f3-L, FGOALS-g3, FIO-ESM-2-0, and NESM3) from China for the period of 1979–2014. The table in the upper left shows the corresponding linear trend of the sea ice drift speed [cm s^{-1} (10 yr)$^{-1}$]. Asterisk indicates the confidence level of the trend reaches 95%. The domain of the spatial mean is the same as the SCICEX domain, which is marked as the red box in Fig. 1a.

strength of BG and TDS as that in the observation in spring. In autumn, two of the nine models show a similar BG extent as that in the observation while five of the nine models show a larger BG extent and stronger BG magnitude than that in the observation.

(2) For the relationship among the spatial patterns of sea ice drift, near-surface wind, and surface ocean current, seven of the nine models agree with the observation/reanalysis in the sense that the spring (MAM) sea ice drift pattern is in good agreement with the near-surface wind pattern. Six of the nine models also show that the sea ice drift pattern is in good agreement with the surface ocean current pattern. However, they are not in good agreement in the observation/reanalysis. In autumn (SON), the relationship among the spatial patterns of sea ice drift, near-surface wind, and surface ocean current is similar to that in spring for all nine models except CIESM, in which the sea ice drift pattern does not match well with near-surface wind in autumn.

(3) The observation/reanalysis shows that the sea ice drift speed significantly increased over most of the Arctic in spring and autumn from 1979 to 2014. These sea ice drift speed changes are not wind-driven because no significant near-surface wind speed changes are associated with them. Besides, the observational sea ice drift speed changes are only weakly linked with the surface ocean current speed changes. Of the nine models, only FGOALS-f3-L, FGOALS-g3, and NESM3 partly capture the significant spring sea ice drift acceleration over the Arctic. Areas with the significant near-surface wind speed and surface ocean current speed changes are also small and rarely co-located with the sea ice drift speed changes in all nine models except for NESM3.

(4) Compared with the observation, more than half of the models (five out of nine) overestimate the Arctic basin-wide climatological sea ice drift speed in all 12 months during 1979–2014. One model (FGOALS-g3), in contrast, underestimates the sea ice drift speed in all 12 months. The simulated peaks and troughs of the sea ice drift speed seasonal cycle in most of the models do not agree with the observation.

(5) For the trend of the Arctic basin-wide mean sea ice drift speed from 1979 to 2014, eight of the nine models do not capture the observational significant sea ice drift speed increase in both spring and autumn. Only FGOALS-g3 captures a weak, but significant sea ice drift speed increase in both spring and autumn.

Since both the BG and TSD patterns of the nine models in the normal mean sea ice drift field (averaged over all the years from 1979–2014) are close to these patterns in the sea ice field averaged over the years with the AO index being less than –1.0 (Figs. S2 and S3 in the electronic supplementary material), the differences in BG and TSD depiction ability of the nine models are associated with their BG and TSD depiction ability in the negative phase of the AO. The missing widespread sea ice drift speed acceleration across the Arctic in the nine models indicates that improvements in the formulation and parameterization of sea ice dynamics are needed in these models, such as the sea ice rheology.

The uncertainty in NSIDC Pathfinder sea ice drift

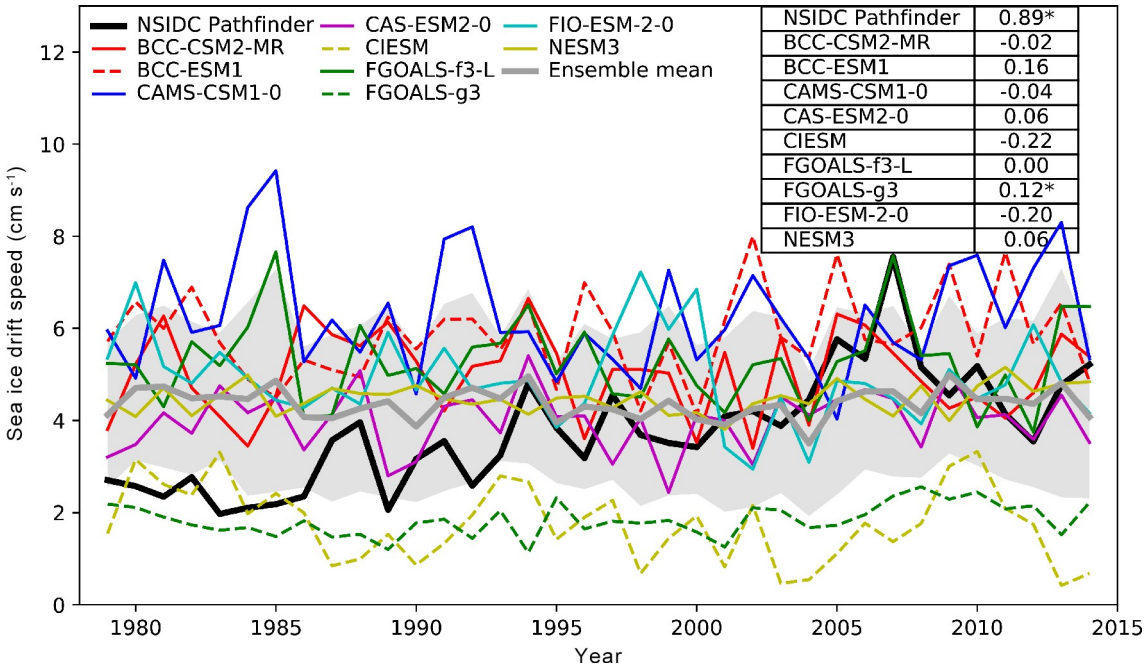

Fig. 12. Same as that in Fig. 11, but for autumn (SON).

speed is noteworthy. Based on daily sea ice drift speed, Docquier et al. (2017) showed that the Arctic basin-wide sea ice drift speed seasonal evolution in NSDIC Pathfinder is different from that in the Arctic buoy observation. According to the daily or 12-hourly Arctic buoy observations, sea ice drift speed peaks in September and troughs in March (Olason and Notz, 2014; Docquier et al., 2017; Tandon et al., 2018).

The source of Arctic sea ice drift is different from the sources of near-surface wind and surface ocean current in our study. These differences may introduce uncertainty in the obtained relationship between the sea ice drift, near-surface wind, and surface ocean current. In order to investigate this uncertainty, we changed the near-surface wind data source from ERA-Interim to NCEP/NCAR Reanalysis (NCEP-R1) because it is one of the sources to calculate the NSIDC Pathfinder sea ice motion. We also changed the surface ocean current source from ORAS4 to Pan-Arctic Ice Ocean Modeling and Assimilation System (PIOMAS) because PIOMAS uses the NCEP-R1 as the atmospheric forcing, including the near-surface wind. After the near-surface and surface ocean current data sources were changed, the relationship between the Arctic sea ice drift and the near-surface wind remained the same (Figs. S4–S8 in the electronic supplementary material). The relationship between the Arctic sea ice drift speed and surface ocean current speed trend is much better after the sources of near-surface wind and surface ocean current were changed (Figs. S7 and S8 in the electronic supplementary material). Therefore, the uncertainty in the relationship between the Arctic sea ice drift and the surface ocean current is large.

In the future, investigation of the air–ice and ice–ocean drag coefficient differences among the models could be helpful to explain the differences in sea ice drift-wind and sea ice drift-ocean current relationships among the models (Tandon et al., 2018). In addition, the temporal variations of the relationship between sea ice drift speed, near-surface wind, and surface ocean current in the models also need to be investigated in the future as the influence of wind and ocean current on the Arctic sea ice drift change has decadal variability (Spreen et al., 2011; Kwok et al., 2013).

Acknowledgements. This research is supported by the National Key R&D Program of China (Grant No. 2018YFA0605904) and the National Natural Science Foundation of China (Grant No. 41701411).

Electronic supplementary material: Supplementary material is available in the online version of this article at https://doi.org/10.1007/s00376-021-1153-4.

REFERENCES

Årthun, M., I. H. Onarheim, J. Dörr, and T. Eldevik, 2021: The seasonal and regional transition to an ice-free arctic. *Geophys. Res. Lett.*, **48**, e2020GL090825, https://doi.org/10.1029/2020GL090825.

Balmaseda, M. A., K. Mogensen, and A. T. Weaver, 2013: Evaluation of the ECMWF ocean reanalysis system ORAS4. *Quart. J. Roy. Meteor. Soc.*, **139**, 1132–1161, https://doi.org/10.1002/qj.2063.

Bao, Y., Z. Y. Song, and F. L. Qiao, 2020: FIO-ESM version 2.0: Model description and evaluation. *J. Geophys. Res.*, **125**, e2019JC016036, https://doi.org/10.1029/2019JC016036.

Berrisford, P., and Coauthors, 2011: The ERA-Interim archive version 2.0. ERA Rep. European Centre for Medium Range Weather Forecast

Cao, J., and Coauthors, 2018: The NUIST Earth System Model

(NESM) version 3: Description and preliminary evaluation. *Geoscientific Model Development*, **11**, 2975–2993, https://doi.org/10.5194/gmd-11-2975-2018.

Chen, S. Z., J. P. Liu, Y. F. Ding, Y. Y. Zhang, X. Cheng, and Y. Y. Hu, 2021: Assessment of snow depth over Arctic sea ice in CMIP6 models using satellite data. *Adv. Atmos. Sci.*, **38**, 168–186, https://doi.org/10.1007/s00376-020-0213-5.

Colony, R., and A. S. Thorndike, 1984: An estimate of the mean field of Arctic sea ice motion. *J. Geophys. Res.*, **89**, 10 623–10 629, https://doi.org/10.1029/JC089iC06p10623.

Davy, R., and S. Outten, 2020: The arctic surface climate in CMIP6: Status and developments since CMIP5. *J. Climate*, **33**, 8047–8068, https://doi.org/10.1175/JCLI-D-19-0990.1.

de Vernal, A., C. Hillaire-Marcel, C. Le Duc, P. Roberge, C. Brice, J. Matthiessen, R. F. Spielhagen, and R. Stein, 2020: Natural variability of the Arctic Ocean sea ice during the present interglacial. *Proceedings of the National Academy of Sciences of the United States of America*, **117**, 26 069–26 075, https://doi.org/10.1073/pnas.2008996117.

Docquier, D., F. Massonnet, A. Barthélemy, N. F. Tandon, O. Lecomte, and T. Fichefet, 2017: Relationships between Arctic sea ice drift and strength modelled by NEMO-LIM3.6. *The Cryosphere*, **11**, 2829–2846, https://doi.org/10.5194/tc-11-2829-2017.

Gui, D. W., R. B. Lei, X. P. Pang, J. K. Hutchings, G. Y. Zuo, and M. X. Zhai, 2020: Validation of remote-sensing products of sea-ice motion: A case study in the western Arctic Ocean. *J. Glaciol.*, **66**, 807–821, https://doi.org/10.1017/jog.2020.49.

Guo, Y. Y., and Coauthors, 2020a: Simulation and improvements of oceanic circulation and sea ice by the coupled climate system model FGOALS-f3-L. *Adv. Atmos. Sci.*, **37**, 1133–1148, https://doi.org/10.1007/s00376-020-0006-x.

Guo, Y. Y., Y. Q. Yu, P. F. Lin, H. L. Liu, B. He, Q. Bao, S. W. Zhao, and X. W. Wang, 2020b: Overview of the CMIP6 historical experiment datasets with the climate system model CAS FGOALS-f3-L. *Adv. Atmos. Sci.*, **37**, 1057–1066, https://doi.org/10.1007/s00376-020-2004-4.

Jin, J. B., and Coauthors, 2021: CAS-ESM2.0 model datasets for the CMIP6 flux-anomaly-forced model intercomparison project (FAFMIP). *Adv. Atmos. Sci.*, **38**, 296–306, https://doi.org/10.1007/s00376-020-0188-2.

Keen, A., and Coauthors, 2021: An inter-comparison of the mass budget of the Arctic sea ice in CMIP6 models. *The Cryosphere*, **15**, 951–982, https://doi.org/10.5194/tc-15-951-2021.

Kwok, R., G. Spreen, and S. Pang, 2013: Arctic sea ice circulation and drift speed: Decadal trends and ocean currents. *J. Geophys. Res.*, **118**, 2408–2425, https://doi.org/10.1002/jgrc.20191.

Lei, R. B., D. W. Gui, J. K. Hutchings, J. Wang, and X. P. Pang, 2019: Backward and forward drift trajectories of sea ice in the northwestern Arctic Ocean in response to changing atmospheric circulation. *International Journal of Climatology*, **39**, 4372–4391, https://doi.org/10.1002/joc.6080.

Lin, Y. L., and Coauthors, 2020: Community integrated earth system model (CIESM): Description and evaluation. *Journal of Advances in Modeling Earth Systems*, **12**, e2019MS002036, https://doi.org/10.1029/2019MS002036.

Lindsay, R., M. Wensnahan, A. Schweiger, and J. Zhang, 2014: Evaluation of Seven Different Atmospheric Reanalysis Products in the Arctic. *J. Climate*, **27**, 2588–2606, https://doi.org/10.1175/JCLI-D-13-00014.1.

Long, M. Y., L. J. Zhang, S. Y. Hu, and S. M. Qian, 2021: Multi-aspect assessment of CMIP6 models for Arctic sea ice simulation. *J. Climate*, **34**, 1515–1529, https://doi.org/10.1175/JCLI-D-20-0522.1.

Notz, D., and Coauthors, 2020: Arctic sea ice in CMIP6. *Geophys. Res. Lett.*, **47**, e2019GL086749, https://doi.org/10.1029/2019GL086749.

Olason, E., and D. Notz, 2014: Drivers of variability in Arctic sea-ice drift speed. *J. Geophys. Res.*, **119**, 5755–5775, https://doi.org/10.1002/2014JC009897.

Petty, A. A., J. K. Hutchings, J. A. Richter-Menge, and M. A. Tschudi, 2016: Sea ice circulation around the Beaufort Gyre: The changing role of wind forcing and the sea ice state. *J. Geophys. Res.*, **121**, 3278–3296, https://doi.org/10.1002/2015JC010903.

Pu, Y., and Coauthors, 2020: CAS FGOALS-g3 model datasets for the CMIP6 scenario model intercomparison project (ScenarioMIP). *Adv. Atmos. Sci.*, **37**, 1081–1092, https://doi.org/10.1007/s00376-020-2032-0.

Rampal, P., J. Weiss, and D. Marsan, 2009: Positive trend in the mean speed and deformation rate of Arctic sea ice, 1979-2007. *J. Geophys. Res.*, **114**, C05013, https://doi.org/10.1029/2008JC005066.

Rampal, P., J. Weiss, C. Dubois, and J. M. Campin, 2011: IPCC climate models do not capture Arctic sea ice drift acceleration: Consequences in terms of projected sea ice thinning and decline. *J. Geophys. Res.*, **116**, C00D07, https://doi.org/10.1029/2011JC007110.

Ren, Y.-J., Y. Xiao, and B. Zhou, 2021: Simulation and projection of Arctic sea ice and climate by BCC-CSM2-MR. *Climate Change Research*, **17**, 58–69, https://doi.org/10.12006/j.issn.1673-1719.2019.168. (in Chinese with English abstract)

Rong, X. Y., and Coauthors, 2018: The CAMS climate system model and a basic evaluation of its climatology and climate variability simulation. *Journal of Meteorological Research*, **32**, 839–861, https://doi.org/10.1007/s13351-018-8058-x.

Rong, X. Y., J. Li, H. M. Chen, J. Z. Su, L. J. Hua, Z. Q. Zhang, and Y. F. Xin, 2021: The CMIP6 historical simulation datasets produced by the climate system model CAMS-CSM. *Adv. Atmos. Sci.*, **38**, 285–295, https://doi.org/10.1007/s00376-020-0171-y.

Rothrock, D. A., D. B. Percival, and M. Wensnahan, 2008: The decline in arctic sea-ice thickness: Separating the spatial, annual, and interannual variability in a quarter century of submarine data. *J. Geophys. Res.*, **113**, C05003, https://doi.org/10.1029/2007JC004252.

Serreze, M. C., and J. Stroeve, 2015: Arctic sea ice trends, variability and implications for seasonal ice forecasting. *Philosophical Transactions of the Royal Society A: Mathematical, Physical and Engineering Sciences*, **373**, 20140159, https://doi.org/10.1098/rsta.2014.0159.

Shen, Z. L., A. M. Duan, D. L. Li, and J. X. Li, 2021: Assessment and ranking of climate models in arctic sea ice cover simulation: From CMIP5 to CMIP6. *J. Climate*, **34**, 3609–3627, https://doi.org/10.1175/JCLI-D-20-0294.1.

Shu, Q., Q. Wang, Z. Y. Song, F. L. Qiao, J. C. Zhao, M. Chu, and X. F. Li, 2020: Assessment of sea ice extent in CMIP6 with comparison to observations and CMIP5. *Geophys. Res. Lett.*, **47**, e2020GL087965, https://doi.org/10.1029/2020GL087965.

Smith, A., A. Jahn, and M. Y. Wang, 2020: Seasonal transition dates can reveal biases in Arctic sea ice simulations. *The Cryosphere*, **14**, 2977–2997, https://doi.org/10.5194/tc-14-2977-2020.

Spreen, G., R. Kwok, and D. Menemenlis, 2011: Trends in Arctic sea ice drift and role of wind forcing: 1992–2009. *Geophys. Res. Lett.*, **38**, L19501, https://doi.org/10.1029/2011GL048970.

Stroeve, J. C., J. Maslanik, M. C. Serreze, I. Rigor, W. Meier, and C. Fowler, 2011: Sea ice response to an extreme negative phase of the Arctic Oscillation during winter 2009/2010. *Geophys. Res. Lett.*, **38**, L02502, https://doi.org/10.1029/2010GL045662.

Stroeve, J. C., M. C. Serreze, M. M. Holland, J. E. Kay, J. Malanik, and A. P. Barrett, 2012: The Arctic's rapidly shrinking sea ice cover: A research synthesis. *Climatic Change*, **110**, 1005–1027, https://doi.org/10.1007/s10584-011-0101-1.

Sumata, H., T. Lavergne, F. Girard-Ardhuin, N. Kimura, M. A. Tschudi, F. Kauker, M. Karcher, and R. Gerdes, 2014: An intercomparison of Arctic ice drift products to deduce uncertainty estimates. *J. Geophys. Res.*, **119**, 4887–4921, https://doi.org/10.1002/2013JC009724.

Sumata, H., R. Gerdes, F. Kauker, and M. Karcher, 2015: Empirical error functions for monthly mean Arctic sea-ice drift. *J. Geophys. Res.*, **120**, 7450–7475, https://doi.org/10.1002/2015JC011151.

Sun, H. C., and G. Q. Zhou, 2010: An arctic sea ice simulation using an ocean-ice coupled model. *Atmos. Ocean. Sci. Lett.*, **3**, 219–223, https://doi.org/10.1080/16742834.2010.11446874.

Tandon, N. F., P. J. Kushner, D. Docquier, J. J. Wettstein, and C. Li, 2018: Reassessing sea ice drift and its relationship to long-term Arctic sea ice loss in coupled climate models. *J. Geophys. Res.*, **123**, 4338–4359, https://doi.org/10.1029/2017JC013697.

Tschudi, M., C. Fowler, J. Maslanik, J. S. Stewart, and W. N. Meier, 2016: Polar Pathfinder daily 25 km EASE-Grid Sea Ice motion vectors, version 3. NASA National Snow and Ice Data Center Distributed Active Archive Center, accessed April 2021., https://doi.org/10.5067/O57VAIT2AYYY.

Vihma, T., P. Tisler, and P. Uotila, 2012: Atmospheric forcing on the drift of Arctic sea ice in 1989–2009. *Geophys. Res. Lett.*, **39**, L02501, https://doi.org/10.1029/2011GL050118.

Wang, S., J. Su, M. Chu, and X. L. Shi, 2020: Comparison of simulation results of the Arctic sea ice by BCC_CSM: CMIP5 and CMIP6 historical experiments. *Haiyang Xuebao*, **42**, 49–64, https://doi.org/10.3969/j.issn.0253-4193.2020.05.006. (in Chinese with English abstract)

Wu, T. W., and Coauthors, 2019: The Beijing climate center climate system model (BCC-CSM): The main progress from CMIP5 to CMIP6. *Geoscientific Model Development*, **12**, 1573–1600, https://doi.org/10.5194/gmd-12-1573-2019.

Wu, T. W., and Coauthors, 2020: Beijing climate center earth system model version 1 (BCC-ESM1): Model description and evaluation of aerosol simulations. *Geoscientific Model Development*, **13**, 977–1005, https://doi.org/10.5194/gmd-13-977-2020.

Xu, S. M., and Coauthors, 2013: Simulation of sea ice in FGOALS-g2: Climatology and late 20th century changes. *Adv. Atmos. Sci.*, **30**, 658–673, https://doi.org/10.1007/s00376-013-2158-4.

Zhang, F. Y., X. P. Pang, R. B. Lei, M. X. Zhai, X. Zhao, and Q. Q. Cai, 2021: Arctic sea ice motion change and response to atmospheric forcing between 1979 and 2019. *International Journal of Climatology*, 1–23, https://doi.org/10.1002/joc.7340.

Zhou, T. J., L. W. Zou, and X. L. Chen, 2019: Commentary on the coupled model intercomparison project phase 6 (CMIP6). *Climate Change Research*, **15**, 445–456, https://doi.org/10.12006/j.issn.1673-1719.2019.193. (in Chinese with English abstract)